MATERIALS CHEMISTRY FRONTIERS

CCS 中国化学会 CHINESE CHEMICAL SOCIETY

ICCAS

ROYAL SOCIETY OF CHEMISTRY

REVIEW

View Article Online
View Journal | View Issue

Cite this: *Mater. Chem. Front.*, 2021, **5**, 5516

Recent advances on electrocatalytic fixation of nitrogen under ambient conditions

Bin Wu,[ab] Yichao Lin,[*ab] Xuezhen Wang*[ab] and Liang Chen[*ab]

Received 17th February 2021,
Accepted 12th May 2021

DOI: 10.1039/d1qm00269d

rsc.li/frontiers-materials

As one of the most important chemicals for human beings, ammonia is produced by the well-known Haber–Bosch process, which consumes tremendous amounts of energy and simultaneously results in unwanted emissions. Very recently, the electrochemical nitrogen reduction reaction (e-NRR) emerged as an intriguing technique for nitrogen fixation, which can be driven by sustainable power sources, such as solar and wind energy. Moreover, ammonia produced by e-NRR can be realized under mild conditions. Nevertheless, the electrochemical nitrogen fixation suffers from a low yield of ammonia due to the scaling relations of intermediates and competing hydrogen evolution. In addition, the progress in the e-NRR is also hindered by unreliable ammonia measurements. In this review, we summarize and discuss the recently reported e-NRR electrocatalysts, and highlight the e-NRR mechanisms and promising strategies for the rational design of e-NRR electrocatalysts. Importantly, the nitrogen contaminations, which resulted in false positive results, are also mentioned and a rigorous ammonia detection method is presented. Moreover, the current challenges and prospects for e-NRR catalysis are discussed. This review gives a fresh impetus to the rational design of high-performance e-NRR electrocatalysts.

1. Introduction

Ammonia is a key precursor for synthetic fertilizers, and has revolutionized the food supply for human beings.[1,2] The ever-increasing population of the world in the past century is directly or indirectly related to the artificial synthesis of ammonia. In addition, ammonia also serves as a key component for some nonbiological uses, such as dyes, explosives and resins.[3] Notably, anhydrous ammonia can be used as a very promising hydrogen carrier and renewable fuel for solid oxide fuel cells (SOFCs) owing to its high hydrogen density.[4] Although N_2 is very abundant in the atmosphere (78% by volume), the extremely high bond energy of N≡N (940.95 kJ mol^{-1}) makes the fixation of N_2 at ambient temperature and pressure very challenging.

[a] *Ningbo Institute of Materials Technology and Engineering, Chinese Academy of Sciences, Ningbo, Zhejiang 315201, P. R. China. E-mail: yclin@nimte.ac.cn, wangxzh@nimte.ac.cn, chenliang@nimte.ac.cn*

[b] *University of Chinese Academy of Sciences, Beijing 100049, P. R. China*

Yichao Lin

Yichao Lin obtained his BS in materials science and engineering from Xi'an University of Science and Technology in 2009 and PhD in physical chemistry of materials from Ningbo Institute of Materials Technology and Engineering, Chinese Academy of Science in 2015. He then worked as a post-doctoral fellow at the same institute. In 2016–2017, he spent 8 months in Rutgers University as a visiting scholar in Jing Li group. Currently, he is an associate professor in Ningbo Institute of Materials Technology and Engineering, Chinese Academy of Science. His current research is focused on the design and synthesis electrocatalysts that are relevant to energy storage and conversion.

Liang Chen

Liang Chen received his BS in applied chemistry from Nanjing University in 2001 and PhD from the Department of Chemical Engineering at the University of Pittsburgh and National Energy Technology Lab in 2006. Currently, he is a professor at Ningbo Institute of Materials Technology and Engineering, CAS. His research is focused on the design and development of novel porous materials for gas sorption, separation and catalysis.

Currently, the synthesis of ammonia in industrial plants is mainly based on the well-known Haber–Bosch process, which was established in 1908. The annual ammonia production by the industrial Haber–Bosch process is 150 million metric tons.[5] The main drawbacks of the Haber–Bosch process are high energy consumption and large amounts of emission, since the reaction requires both high temperature (300–500 °C) and pressure (150–300 atm), which roughly consumes ~2% of the world's energy supply and generates 400 million metric tons of fossil fuel-derived CO_2 annually.[6–8]

Therefore, it is highly desired to develop an alternative approach with friendly operating conditions, low energy consumption and minimal CO_2 emissions. Many efforts have been devoted to the biological N_2 fixation using nitrogenase, which is more energy efficient than the Haber–Bosch process. However, the biological N_2 fixation is limited by the sluggish kinetics and instability of nitrogenase.[9–11] Recently, an electrochemical nitrogen reduction reaction (e-NRR) under mild conditions emerged as a promising technology for nitrogen fixation.[12–16] The electricity required for the e-NRR can be generated from sustainable solar and wind energy.[17] However, it is worth noting that the hydrogen evolution reaction (HER) equilibrium potentials are very close to the e-NRR equilibrium potentials in both acidic and alkaline electrolytes.[18] Accordingly, the HER process strongly competes with the e-NRR on the cathode. Moreover, the e-NRR with multiple proton–electron coupling and transferring reactions exhibits a more sluggish kinetic than the HER with only two-electron transfer. In recent years, many efforts have been made to develop highly-efficient e-NRR electrocatalysts. However, the reported ammonia yield rates are still in the ppm scale. Moreover, many electrocatalysts with unreliable detection of ammonia may be misleading to the researchers for designing optimal catalysts for the e-NRR. Thus, developing strategies to fabricate e-NRR electrocatalysts with high-performance and reliable operation methods for accurate ammonia detection are definitely urgent in the e-NRR research community. In this review, we first present the well accepted e-NRR mechanisms, as well as experimental evidences, in order to provide an in-depth understanding of the e-NRR process at the atomistic level. In the second part, we summarize, classify and discuss the recently reported e-NRR electrocatalysts, and put emphasis on some promising strategies for improving e-NRR performance. Finally, we highlight some challenges and perspectives for the design of e-NRR electrocatalysts.

2. Possible mechanism of the e-NRR

In general, the reported e-NRR process can be classified into two pathways: (i) dissociative pathway, and (ii) associative pathway (Fig. 1a–c).[19] In the dissociative pathway, the triple N≡N bond of dinitrogen is firstly cleaved, and subsequently a single N atom is adsorbed on the electrocatalyst surface. Hydrogenations of the N atom occur in the following steps to release an NH_3 molecule. In contrast, in the associative pathway, dinitrogen is adsorbed on the catalyst in an end-on or side-on manner. In the end-on manner, one proton is adsorbed on the N atom far away from the surface, and simultaneously one electron is transferred to the N atom. After that, hydrogenations on the two N atoms follow two possible processes: distal process and alternating process. In the distal process, hydrogenation preferentially takes place on the N atom far away from the surface of catalyst, while in the alternating process the hydrogenation of end-on dinitrogen takes place alternately. In the side-on manner, the adsorbed dinitrogen is hydrogenated alternately to realize the splitting of a N≡N bond. This mechanism is the so-called enzymatic pathway. Nørskov and coworkers theoretically calculated the trends in catalytic activity over a range of transition metals based on an associative or dissociative pathway.[20] The results revealed that the most active e-NRR metals are Mo, Fe, Rh and Ru. However, the competing HER on these metals greatly reduce their faradaic efficiency. In contrast, the early transition metals, including Sc, Y, Ti and Zr, exhibited stronger N-adatoms adsorption than

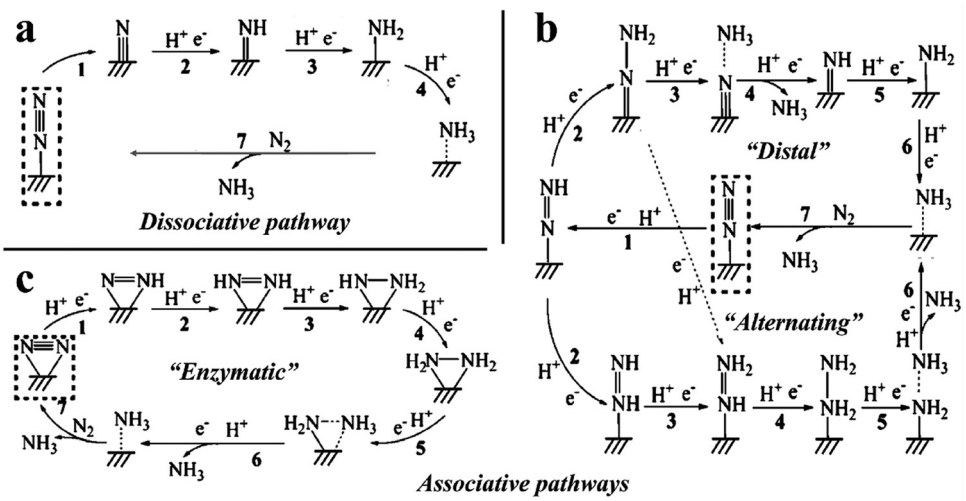

Fig. 1 Schematic depiction of possible NRR mechanisms of (a) dissociative pathway, and (b and c) associative pathways. Reproduced with permission.[26] Copyright 2016 American Chemical Society.

H-adatoms. Recently, some advanced experimental techniques were employed to monitor the intermediates helping to reveal the possible e-NRR mechanism. For example, Yao *et al.* employed a powerful surface-enhanced infrared absorption spectroscopy (SEIRAS) technique to probe the e-NRR mechanism on the Au surface.[21] The resulting spectra demonstrated the existence of N_2H_y ($2 \leq y \leq 4$) adsorbate with bands of the H–N–H bending at 1453 cm^{-1}, the $-NH_2$ wagging at 1298 cm^{-1}, and the N–N stretching at 1109 cm^{-1} at a potential below 0 V *vs.* RHE, suggesting an associative pathway of the e-NRR on the Au surface. The authors further used the SEIRAS technique combined with differential electrochemical mass spectrometry (DEMS) to investigate the e-NRR process on Rh.[22] Based on the experimental evidence, they proposed that the e-NRR on Rh follows a novel pathway involving two steps: an electrochemical reduction of N_2 to N_2H_2 on the Rh surface and a chemical-decomposition of N_2H_2 to NH_3 and N_2 in electrolyte (Fig. 2a). Likewise, Qiao and coworkers successfully probed the N_2H_2 intermediates on *in situ* fragmented bismuth nanoparticles by using online DEMS.[23] In their study, no *m*/*z* signal at 27, 31, and 33 was detected, indicating the absence of N_2H_4 intermediate. But the presence of an *m*/*z* signal at 30 confirmed the formation of N_2H_2 during the e-NRR process. N_2H_2 intermediates together with the detected NH_3 varying with the applied voltage suggested that the e-NRR might follow an associative pathway on the *in situ* fragmented bismuth nanoparticles.

Recently, the e-NRR process on transition metal nitrides was proposed to follow the Mars–van Krevelen (MvK) mechanism (Fig. 2b).[24] In this mechanism, a vacancy is firstly created on a lattice N atom after the protonation of the nitrogen atom on the surface of transition metal nitrides (TMNs). After that, dinitrogen from the electrolyte refills the N vacancy, and is further hydrogenated to release two NH_3 molecules and regenerate the N vacancy. Nevertheless, the nitride catalyst itself could decompose to ammonia if the migration of the N-vacancy from the surface to the bulk rather than the regeneration of N-vacancy with dinitrogen.[25] Importantly, the sustainable catalytic reaction may cease if the surface vacancy gets poisoned by O, H, or OH.

3. Noble metal-based e-NRR catalysts

3.1 Au-Based materials

Bao *et al.* reported that tetrahexahedral Au nanorods enclosed by {730} crystal planes possess excellent e-NRR catalytic performance, with a high NH_3 production yield rate of 1.648 μg h^{-1} cm^{-2} and a $N_2H_4{\cdot}H_2O$ production yield rate of 0.102 μg h^{-1} cm^{-2} at −0.2 V *vs.* RHE.[27] The {730} is a stepped facet composed of the (210) and (310) sub-facets which are beneficial for the e-NRR process as revealed by density functional theory (DFT) calculations (Fig. 3a and b). To enhance the effective utilization of expensive Au, the authors further fabricated Au sub-nanoclusters on a TiO_2 support for the e-NRR.[28] As expected, the Au sub-nanoclusters exhibited an effective and stable e-NRR catalytic performance, with significant enhancement in NH_3 production yield (21.4 μg h^{-1} mg_{cat}^{-2}) and faradaic efficiency (8.11%). Moreover, it is feasible to improve the adsorption of N_2 and the first protonation of $*N_2$ by exposing Au high-index facets. For example, Tian *et al.* reported high-index faceted Au nanoparticles (AuNPs) synthesized by a modified seed-mediated method.[29] The AuNPs with multiple high-index facets, such as (553) and (551), exhibited a NH_3 production rate of 9.22 μg h^{-1} cm^{-2} and a high faradaic efficiency of 73.32% at −0.3 V. The DFT calculations revealed that Au(551) and Au(553) possessed a lower energy barrier at the rate determining step (RDS) ($*NN + H^+ + e^- \rightarrow *NNH$) than the Au(110) surface. On the other hand, the competing *H adsorption was suppressed on the Au(553) and Au(551), leaving more active sites for the e-NRR. In additional to exposing high-index facets of Au, tuning the electronic structure of Au is also an effective way to enhance the e-NRR activity. Zheng *et al.* employed a CoO_x layer to modify the local electronic structure of Au nanoparticles.[30] As revealed by the X-ray photoelectron spectroscopy (XPS) analysis, the introduction of the CoO_x layer resulted in the creation of Au^{1+} species on the Au nanoparticles due to the electron transfer from Au^0 to Co^{3+} (Fig. 3c). DFT calculations show that, compared with Au^0, Au^{1+} species has a stronger interaction with the N_2 molecule, and is much more active in catalyzing the e-NRR process *via* reducing the uphill free energy of RDS (Fig. 3d). Besides improving

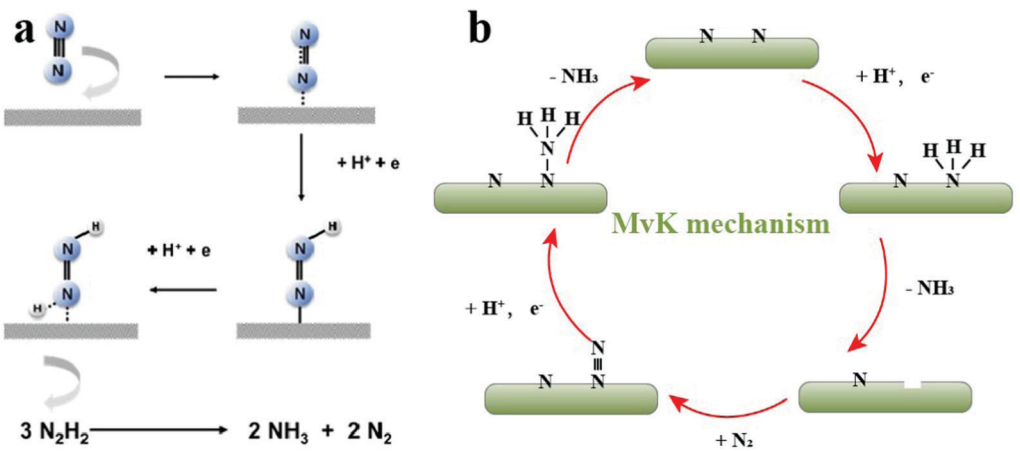

Fig. 2 (a) Schematic description of possible electrochemical pathways for NRR on a Rh surface. Reproduced with permission.[21] Copyright 2020 Wiley-VCH. (b) Schematic depiction of the MvK mechanism.

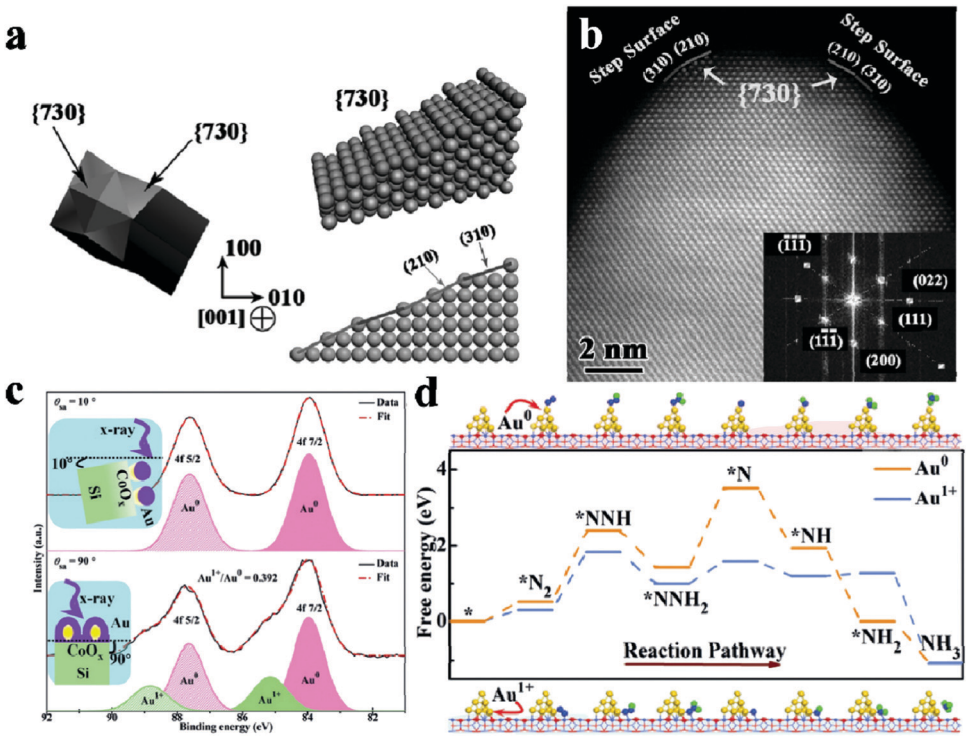

Fig. 3 (a and b) Atomistic level structure of Au THH NR. Reproduced with permission.[27] Copyright 2016 Wiley-VCH. (c) Au 4f spectra of the Au/CoO_x sample. (d) Free energy diagram and optimized geometric structure schematic of the NRR process on Au^0 and Au^{1+} sites of the Au/CoO_x sample following the distal pathway. Reproduced with permission.[30] Copyright 2019 Wiley-VCH.

the intrinsic Au catalytic activity, it is also effective to enhance the e-NRR performance by promoting the accessibility to N_2. For instance, Liu *et al.* reported that Au nanoparticles chemically anchored on a two-dimensional Ti_3C_2 surface were highly active toward the e-NRR.[31] The Ti_3C_2 served as an extractor for adsorbing N_2 from air. The synergistic effect on the interface between Au particles and Ti_3C_2 weaken the N≡N bonds and lower the total energy barrier of the e-NRR. Zhang *et al.* reported that heterogeneous Au–Fe_3O_4 nanoparticles can effectively fix nitrogen to NH_3 through the e-NRR.[32] The high e-NNR activity of Au–Fe_3O_4 was attributed to the synergistic effect of the strong N_2 adsorption ability of Fe_3O_4 and the intensive Au–O bonds that can improve the reaction energetics and kinetics. The synergistic effect between Au and supports are also found in MoS_2 nanosheet supported Au,[33] Au/TiO_2 hybrid,[34] and core@shell structured Au@SnO_2.[35] Nazemi *et al.* evaluated the e-NRR performance of hollow Au nanocages (AuHNCs) under ambient conditions.[36] The AuHNCs exhibited great enhancement in ammonia yield rate and faradaic efficiency relative to solid Au nanoparticles of various morphologies (cubes, rods, or spheres), which was ascribed to the increased surface area and confinement effects.

3.2 Pd-Based materials

Wang *et al.* reported an efficient e-NRR catalyst of Pd nanoparticles supported on carbon black, which realized a NH_3 yield rate of ~4.5 μg mg_{Pd}^{-1} h^{-1} and a faradaic efficiency of 8.2% at 0.1 V *vs.* RHE.[37] Based on DFT calculations, they proposed that the *in situ* generated Pd hydride could effectively facilitate the hydrogenation of N_2 to N_2H* *via* a Grotthuss-like hydride transfer pathway. In a further work, Deng *et al.* improved the e-NRR activity of Pd nanoparticles by surface modification using oxygen-rich tannic acid.[38] Zhao *et al.* found that Pd cube nanocatalysts with an exposed (100) facet exhibited higher e-NRR activity than the Pd nanocatalyst with exposed (110) or (111) facets.[39] DFT calculations revealed that the energy barrier for generating NH_3 from *NH_3 or N_2 adsorption on the surface of (100) is lower than that on the (110) or (111) surface. Indeed, the temperature-programmed desorption (TPD) of N_2 experiments indicated a strong N_2 adsorption on the Pd(100) surface. Pd-Based alloys with a porous structure and desired electronic structure were also fabricated for efficient e-NRR catalysis.[40–42] For example, Pang *et al.* synthesized a porous Pd_3Cu_1 alloy with the desired electronic structure for suppressing HER.[40] Zhao *et al.* prepared PdPb nanosponges in which Pb served as an inhibitor for HER, facilitated the adsorption of dinitrogen and decreased the energy barrier of the *NNH intermediate.[42] Ma *et al.* introduced vacancy defects in a PdZn nanocatalyst by an acid-etching strategy.[43] The vacancy defects were proposed to play a vital role in N_2 molecule adsorption and hydrogenation for the e-NRR and simultaneously suppressing the HER. Moreover, the e-NRR catalytic activity of the Pd alloy can be modified by crystal phase engineering.[44] For example, the body-centered cubic (BCC) PdCu nanoparticles were demonstrated to be much more active and selective for ammonia synthesis than face-centered cubic PdCu. Theoretical calculations revealed that the efficient e-NRR catalysis originated from the enhanced

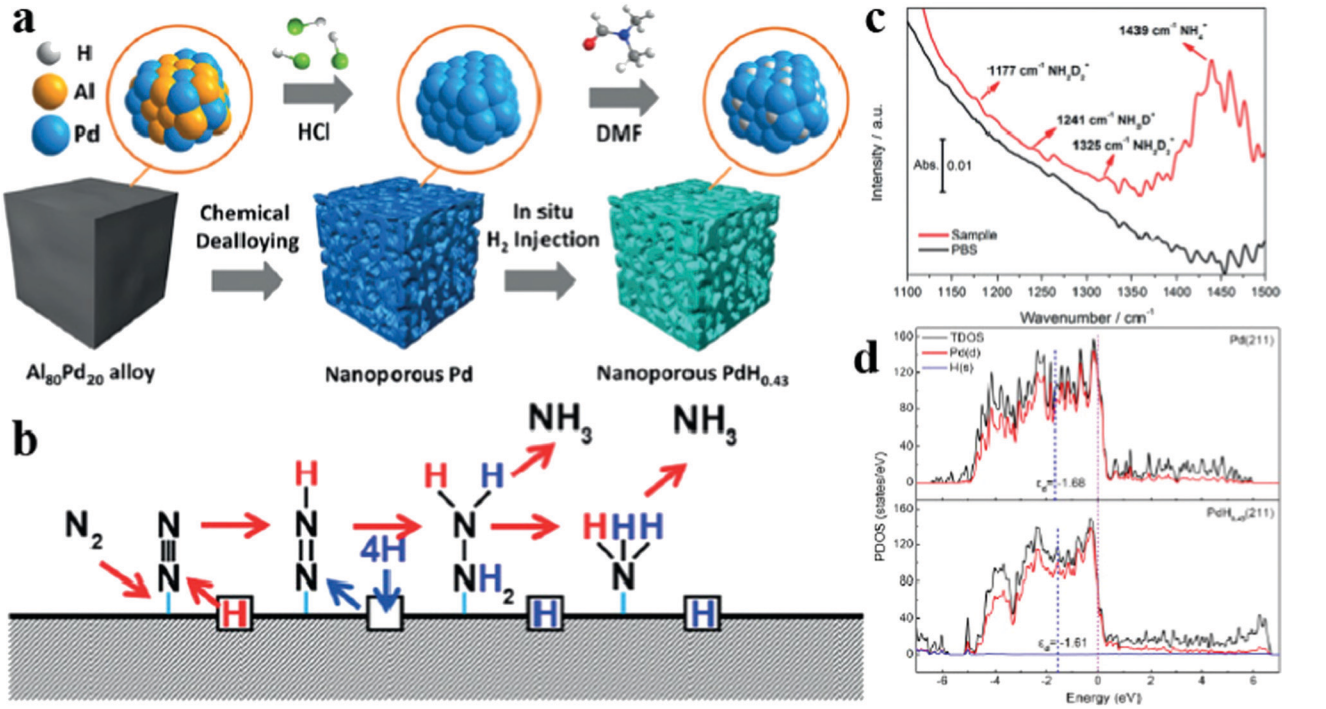

Fig. 4 (a) The fabrication of nanoporous Pd hydride. (b) Proposed lattice hydrogen-involved reaction mechanism for nitrogen reduction on palladium hydride. (c) FTIR spectra of the post-electrolyte with deuterium substituted catalyst. (d) The projected density of states for np-Pd and np-$PdH_{0.43}$. Reproduced with permission.[45] Copyright 2019 Wiley-VCH.

Pd 4d electronic activity in BCC PdCu due to the strong orbital interactions between Pd and adjacent Cu atoms. Hydride treatment for Pd is another effective strategy to lower the Gibbs free-energy (ΔG) of the process of the first protonation step of *NN. Recently, Xu *et al.* reported nanoporous $PdH_{0.43}$ (np-$PdH_{0.43}$) synthesized by chemical dealloying of Pd–Al alloys and *in situ* hydrogen injection methods (Fig. 4a).[45] The hydrogen atoms of $PdH_{0.43}$ participated in activating and binding nitrogen atoms to form e-NRR intermediates, which was confirmed by the FTIR spectra collected in the electrolyte after the e-NRR test using nanoporous Pd deuteride (Fig. 4b and c). In addition, np-$PdH_{0.43}$ has a much lower Gibbs free-energy of *NNH formation (0.65 eV) than np-Pd (0.91 eV) in an alternative enzymatic pathway. Furthermore, the hydrogen injection of np-Pd, leading to the positive shift of d-band center of Pd, also contributed to the stabilization of $*N_xH_y$ intermediates and thus achieved an excellent e-NRR activity with an ammonia yield rate of 20.4 μg h^{-1} mg^{-1} and faradaic efficiency of 43.6% at −0.15 V *vs.* RHE (Fig. 4d).

3.3 Ru-based materials

Ru is located almost at the top of the volcano diagram of Skulasson, thus has become an intriguing electrocatalyst for the e-NRR.[46–54] Yao *et al.* investigated the e-NRR process on Ru thin film by using SEIRAS.[46] The N_2H_x intermediate with the N═N stretching band (~1940 cm^{-1}) was detected during the electroreduction of N_2 in 0.4 M $HClO_4$. It was revealed that the formation rate of N_2H_x intermediate was faster than its consumption, suggesting an effective way to enhance the e-NRR activity by weakening the binding strength of the N_2H_x intermediate on the Ru surface. Theoretically, the bottleneck of Ru metal is its low e-NRR selectivity. Active Ru stepped sites are easily occupied by a high coverage of *H.[55] Such pre-adsorbed *H reduce the active sites available for the protonation of N_2 and hinder the NRR process. Ding *et al.* fabricated Ru cluster-doped CeO_2 nanorods with abundant oxygen vacancies as e-NRR electrocatalysts.[54] The authors proposed that CeO_2 promoted the N_2 adsorption and low-valence Ru nanoclusters were catalytic sites for N_2 activation. Geng *et al.* synthesized Ru single atoms distributed on nitrogen-doped carbon (Ru SACs/NC) by pyrolyzing Ru-containing derivative of ZIF-8 (Fig. 5a), which exhibited a striking e-NRR performance with high ammonia yield rate (120.9 μg mg_{cat}^{-1} h^{-1}) and high faradaic efficiency (29.6%) at −0.2 V *vs.* RHE in 0.05 M H_2SO_4 electrolyte.[50] As shown in Fig. 5b, the intense TPD peak at 340 °C indicated that dinitrogen was adsorbed strongly on Ru single atoms, which might facilitate the sequential e-NRR steps. DFT calculations demonstrated that Ru_1-N_3 and Ru_1-N_4 structures were favorable to the adsorption of N_2 and the protonation of $*N_2$ (Fig. 5c). Similarly, the high e-NRR catalytic activity of Ru single atoms supported on N-doped carbon was also observed by Tao *et al.*[49] In addition, the authors showed that the presence of ZrO_2 in Ru SACs/NC played a vital role in suppressing the competitive HER and thereby enhancing the faradaic efficiency.[49] Peng *et al.* reported single-atomic Ru modified Mo_2CT_x MXene nanosheets as an efficient e-NRR electrocatalyst.[48] DFT calculations combined with *operando* X-ray absorption spectroscopy (XAS) revealed that the Ru single atoms served as the electron back-donation centers for N_2 adsorption and activation, and decreased the energy barrier for *NNH formation. Liu *et al.* presented a Ru@Ti_3C_2MXene

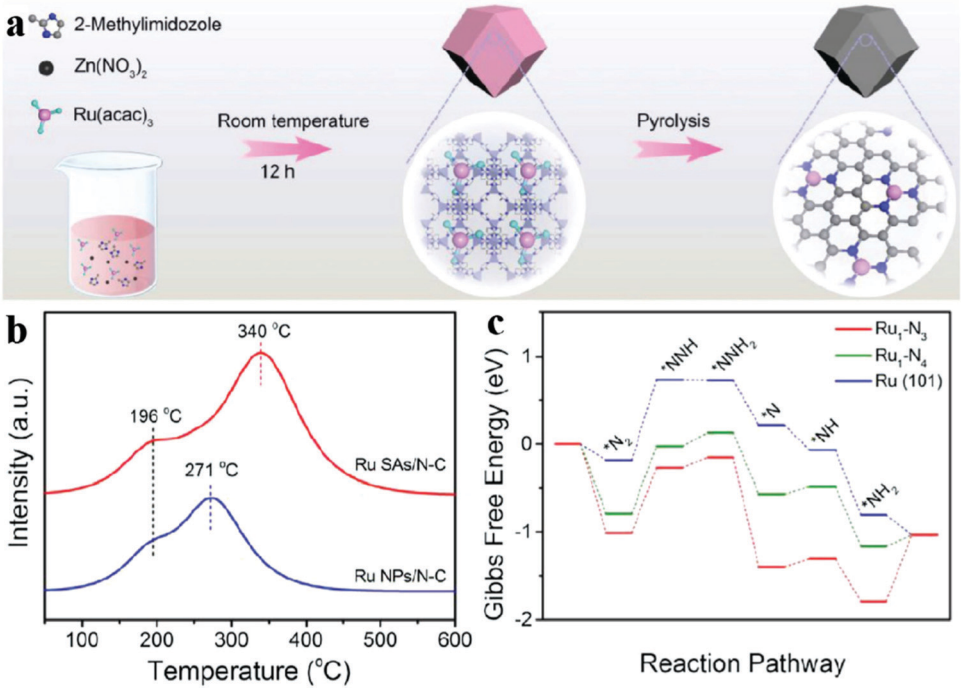

Fig. 5 (a) Scheme of the synthetic route for Ru SAs/N–C. (b) the N_2-TPD profiles of Ru SAs/N–C and Ru NPs/N-C. (c) free energy diagram of the N_2 electrochemical reduction with a distal pathway on Ru_1–N_3, Ru_1–N_4, and Ru(101). * represents an adsorption site. Reproduced with permission.[50] Copyright 2018 Wiley-VCH.

catalyst with uniform distribution of Ru for efficient E-NRR activity. However, the authors did not investigate whether Ru is atomically dispersed or not.[56]

4. Non-noble transition metals

4.1 Mo-Based catalysts

Mo is an important element for catalytic nitrogen fixation in biological systems.[57] The occupied d orbitals of a Mo-based material can back donate electron into antibonding orbitals of N_2 to weaken the triple N≡N bond, which initiate the nitrogen reduction reaction.[58] By far, Mo_2C,[58] MoS_2,[59,60] 1T-MoS_2@Ti_3C_2,[61] $MoSe_2$,[62] and Mo_3Si[63] have been explored for electrocatalytic nitrogen fixation. For instance, Mo_2C nanodots embedded in carbon nanosheets (Mo_2C/C), fabricated by a molten salt synthesis method, delivered an NH_3 yield rate of 11.3 μg h^{-1} $mg_{cat.}^{-1}$ at −0.3 V *vs.* RHE and faradaic efficiency (1.1%) after being coated on hydrophilic carbon cloth.[58] Mo_2C/C coated on hydrophobic cloth exhibited lower ammonia yield rate of 5.7 μg h^{-1} mg^{-1} but higher faradaic efficiency (7.8%) relative to that coated on hydrophilic carbon cloth, which was ascribed to the suppressed HER (Fig. 6a). DFT calculations revealed that Mo_2C confined by oxygen-containing groups in carbon nanosheets showed a high N_2 adsorption energy of −0.842 eV (Fig. 6b and c). In addition, oxygen-doped Mo carbide embedded in N-doped carbon also exhibited comparable e-NRR activity and faradaic efficiency.[64] MoS_2 was also employed to catalyze the e-NRR, which exhibited an intriguing e-NRR activity.[59] DFT calculations suggested that the high e-NRR catalytic activity of MoS_2 originated from the positively charged Mo-edge which played a key role to activate N_2 molecules. Benefitting from the adjacent Mo atom pairs in the holes of the basal plane, Chen *et al.* prepared porous atomic layered MoS_2 by one-step calcination.[60] From DFT calculation results, N_2 can be effectively activated by adjacent Mo atom pairs with a laying-down manner. Han *et al.* reported Mo single atoms dispersed on N-doped carbon (Mo SACs/NC) for an efficient e-NRR. The critical role of Mo–N sites in Mo SACs/NC was confirmed by control experiments. The catalyst with optimized Mo loading exhibited a NH_3 yield rate of ∼34.0 μg h^{-1} $mg_{cat.}^{-1}$ and a faradaic efficiency of ∼14.6% in 0.1 M KOH.[65] Ma *et al.* fabricated both the Mo single atoms and Mo carbide onto N-doped carbon nanotubes to achieve an integrated synergy for the e-NRR.[66] DFT calculations suggested that the Mo single atoms in the catalyst provided large *H coverage for the N_2 activation and facilitated hydrogenation on the e-NRR selective Mo_2C sites.

4.2 Bi-Based materials

Bi is well-known for its low toxicity and environmental benignity.[67] There are two major advantages for using a Bi atom to fix a nitrogen molecule into ammonia. First, the half-filled Bi 6p band electrons can be effectively back donated to the nitrogen empty π* antibonding orbitals, enhancing the adsorption of dinitrogen and thereby improving e-NRR activity.[23] Second, semiconducting Bi can also sufficiently suppress the competitive HER process due to its poor hydrogen adsorption.[68] Hao *et al.* presented a strategy to enhance both the e-NRR activity and selectivity using a Bi nanocrystal catalyst and electrolyte containing potassium cations.[69] The prepared Bi nanocrystals supported on carbon

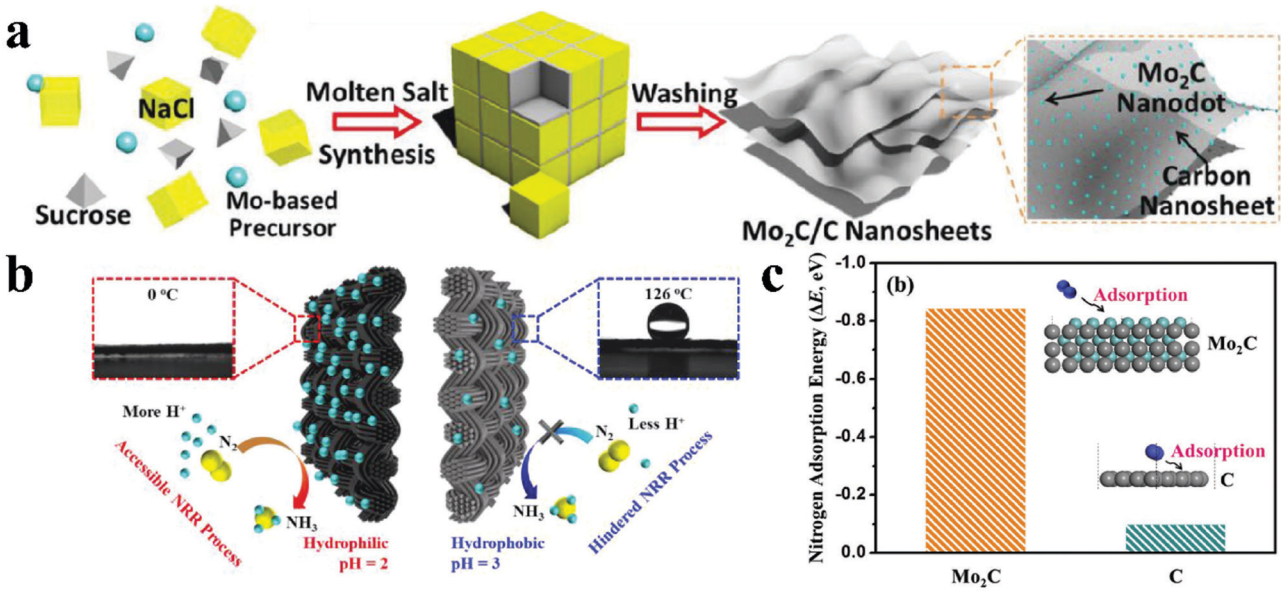

Fig. 6 (a) Scheme of the synthetic route for Mo_2C/C nanosheets. (b) NRR catalytic mechanism depiction of the Mo_2C/C under proton-suppressed and proton-enriched conditions. (c) Nitrogen adsorption energy of Mo_2C and C. Reproduced with permission.[58] Copyright 2018 Wiley-VCH.

black (BiNCs) exhibited an outstanding faradaic efficiency of 66% and a stable ammonia yield of 200 mmol g^{-1} h^{-1} (or 0.05 mmol cm^{-2} h^{-1}) in 1 M K_2SO_4 (pH = 3.5). The projected density of states of *NNH showed that the Bi 6p bands and N 2p orbitals overlapped, suggesting the strong interaction between Bi 6p bands and N 2p orbitals which could stabilize the intermediates and reduce the energy barrier for RDS. The highest barriers of the first protonation step (ΔG_{*NNH}) were reduced both on solvated Bi(012) (from 2.88 eV to 2.42 eV) and Bi(110) (from 2.80 eV to 2.42 eV) surfaces, which was consistent with the red-shift energies of N_{ads} 2p orbitals. Li *et al.* fabricated a mosaic bismuth nanosheet (BiNS) by *in situ* electrochemically reducing the bismuth oxyiodide precursor.[70] Compared with Bi nanoparticles, BiNS exhibited enhanced e-NRR activity, which was ascribed to the high density of edge sites and the p-orbital electron delocalization in the BiNS surface. Xia *et al.* also prepared a Bi nanosheet using a similar approach, and disclosed that N_2 was more likely to adsorb on the surface of the edge plane (010) instead of the basal plane (001) based on DFT calculations.[71] In addition, Yao *et al.* showed that the *in situ* formed fragmented Bi nanoparticles were able to efficiently catalyze N_2 to ammonia in neutral and acidic electrolytes.[23] The catalytic activity of Bi was also improved by introducing a porous carbon coat or support to improve the conductivity.[72]

To improve the intrinsic e-NRR activity of Bi, Wang *et al.* prepared defect-rich Bi nanoplates from Bi_2O_3 by bombardment using low-temperature plasma.[73] The prepared defect-rich Bi nanoplates exhibited much higher e-NRR activity than the crystalline Bi. Fang *et al.* also showed that an amorphous BiNi alloy is much more e-NRR active than its crystalline and metal counterparts.[74] Based on theoretical calculations and experimental analysis, it was proposed that the Ni substitution can modify the electronic structure of Bi and improve the electron transfer. On the other hand, the amorphization created a defect-rich surface and disordered atomic arrangement for effective N_2 adsorption (Fig. 7). In addition, bismuth oxides were also reported as active and stable e-NRR catalysts.[75,76]

4.3 Other transition metal-based catalysts

Zhang *et al.* prepared V_2O_3 nanoparticles uniformly distributed on shuttle-like amorphous carbon (V_2O_3/C) and a VO_2 hollow microsphere as e-NRR catalysts.[77,78] The VO_2 hollow microsphere achieved a high NH_3 yield of 14.85 μg h^{-1} mg^{-1} at −0.7 V in 0.1 M Na_2SO_4. Fang *et al.* synthesized multivalent vanadium oxide nanosheets (mVO_x) with oxygen vacancies.[79] After physically mixing with reduced graphene oxide for improved conductivity, mVO_x exhibited excellent e-NRR activity, which was attributed to the hydrophilicity and oxygen vacancies. Cao *et al.* fabricated bi-Ti^{3+} pairs on anatase TiO_2 by introducing Zr^{4+} with a larger radius into the lattice to remove one oxygen between two adjacent Ti^{4+} sites.[80] Based on DFT calculations and experimental evidence, the adjacent bi-Ti^{3+} pairs were identified as the active centers for efficient N_2 chemisorption and activation. In addition, several individual studies showed that TiO_2 with oxygen defects possessed enhanced e-NRR activity, demonstrating that introducing oxygen defects to the TiO_2 surface is an effective way to improve its e-NRR activity.[81–83] Some other transition metal oxides, such as Y_2O_3 doped zirconia, and Sb_2S_3 nanoparticles anchored on SnO_2, have also been reported to be e-NRR active.[84,85] Sufficient surface-terminated and low-coordinated Fe sites in $FeTe_2$ in a recent report can also adsorb N_2 molecules and activate the NRR process.[86]

5. Metal-free electrocatalysts

5.1 Black phosphorous

Owing to its unique electrochemical properties, black phosphorous (BP) emerged as a hot material in the frontier field of

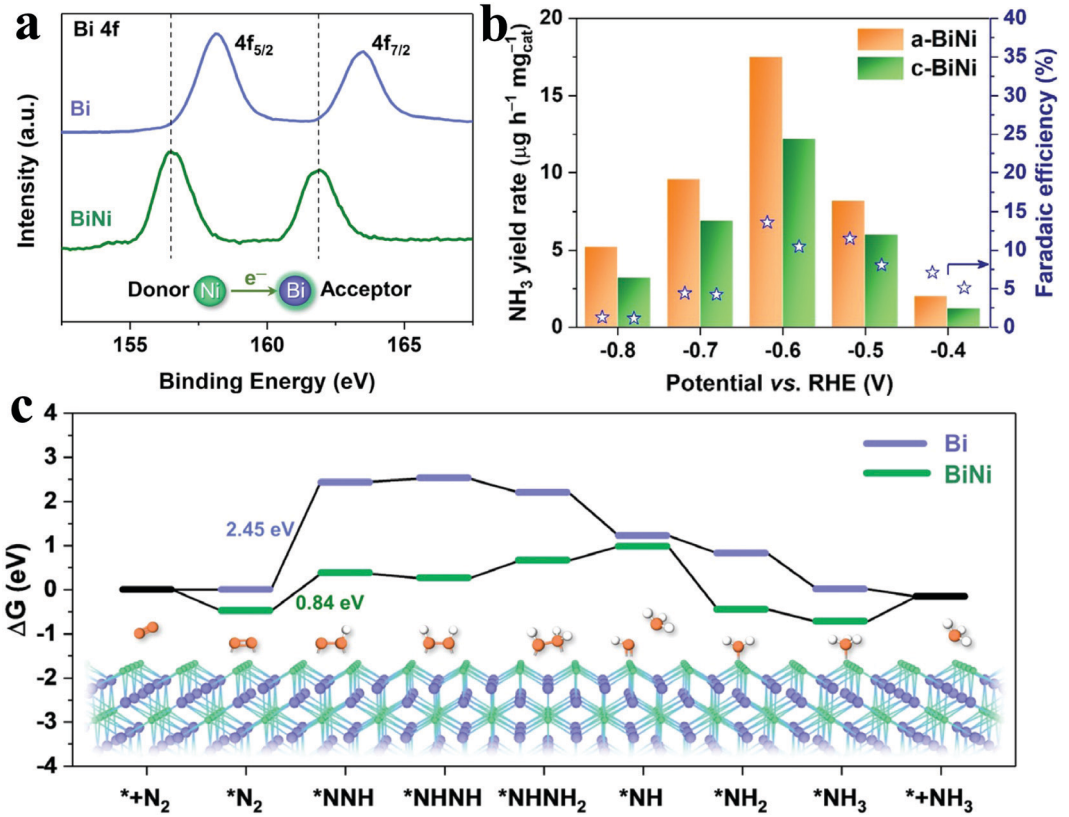

Fig. 7 (a) Bi 4f spectra of Bi and BiNi. (b) NRR activities of a-BiNi and c-BiNi under N_2. (c) Energy diagram of the NRR process on Bi and BiNi. Reproduced with permission.[74] Copyright 2020 Wiley-VCH.

energy storage and conversion.[87,88] Recently, BP was investigated for e-NRR catalysis. For example, Liu *et al.* prepared BP quantum dots (QDs) and dispersed them on black tin oxide (SnO_{2-x}) nanotubes to avoid their agglomeration and improve their electric conductivity.[89] The resulting BP@SnO_{2-x} exhibited impressive e-NRR activity and stability, which was attributed to their synergistic superiority. Wang *et al.* assembled BP QDs on MnO_2 nanosheets for e-NRR catalysts, delivering a high ammonia yield rate of 25.3 μg h^{-1} mg_{cat}^{-1} and faradaic efficiency of 6.7% at −0.5 V *vs.* RHE in 0.1 M Na_2SO_4 electrolyte.[90] XPS characterization revealed the intimate electronic interactions between BP QDs and MnO_2 nanosheets which were beneficial for the e-NRR process. Zhang *et al.* synthesized few-layer BP nanosheets (FL-BP NSs) from commercial bulk BP by using a liquid exfoliation method.[91] Compared with bulk BP and powdery BP, FL-BPNSs exhibited a significantly higher performance with a NH_3 yield rate of 31.37 μg h^{-1} mg_{cat}^{-1} at −0.7 V in 0.01 M HCl electrolyte (Fig. 8a). DFT calculations showed that the active orbitals at the zigzag and diff-zigzag edges of FL-BP NSs were favorable to adsorb N_2 and activate the N≡N triple bond, which facilitate the electroreduction of N_2 to NH_3 *via* an alternating pathway (Fig. 8b).

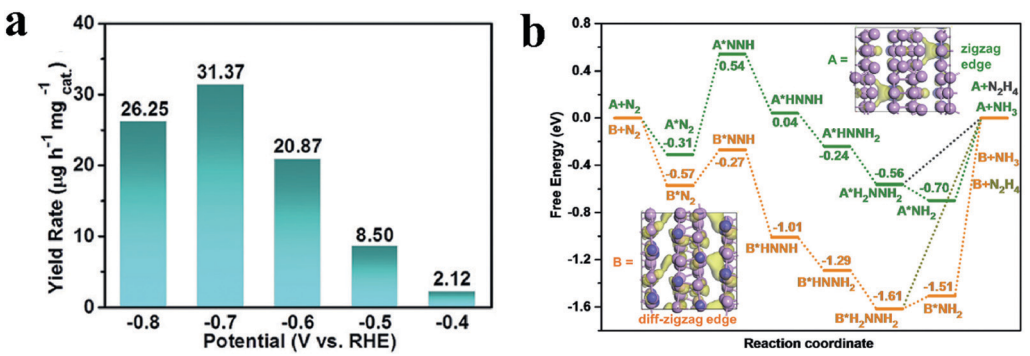

Fig. 8 (a) NH_3 yield rate at various potentials of FL-BP NSs/CF. (b) Reaction pathways and corresponding energy changes of NRR on the zigzag edge (A) and diff-zigzag edge (B) active sites of FL-BP NSs/CF. Reproduced with permission.[91] Copyright 2019 Wiley-VCH.

5.2 Carbon-based materials

5.2.1 Boron doped non-metals. Boron atoms with sp^2 or sp^3 hybridization can effectively interact with N_2 *via* an end-on or side-on pattern, thus have shown great potential for N_2 fixation.[92–96] Specially, for B-doped graphitic carbon, the smaller electronegativity of boron than carbon results in the formation of positively charged B atoms, which possess enhanced N_2 adsorption ability and thus result in the formation of a B–N bond. Yu *et al.* fabricated a series of B-doped graphene (BG) by thermal reduction of a mixture of HBO_3 and graphene oxide.[97] The BG with highest BC_3 content exhibited the best performance, suggesting that BC_3 serves as the major e-NRR electrocatalytic site. Recently, B_4C was also reported to be highly e-NRR catalytically active. Qiu *et al.* prepared B_4C nanosheets *via* liquid exfoliation of bulk B_4C.[98] They showed that the B_4C nanosheet is one of the most active e-NRR catalysts reported by far. DFT calculations revealed that the protonation process on a $B_4C(110)$ surface in the $*NH_2$–$*NH_2$ → $*NH_2$–$*NH_3$ reaction needed to overcome an uphill barrier of 0.34 eV.

5.2.2 N and P doped carbon materials. N-Doped porous carbon with a tuned electronic structure has been extensively investigated in the oxygen reduction reaction (ORR) and CO_2 reduction.[99–101] Recently, Liu *et al.* applied nitrogen doped porous carbons (NPCs) with tunable N species for e-NRR catalysis.[102] The NPC with the highest pyridinic N content exhibited the best e-NRR activity, suggesting that pyridinic N plays a vital role in e-NRR catalysis (Fig. 9). Chen *et al.* showed that the appropriate incorporation of B–N pairs could improve the e-NRR catalytic activity of a carbon matrix.[103] The edge carbon atoms near doped B–N bonds were identified as the active sites. The doping of B–N pairs modified the electronic structures of edge carbon atoms, which was beneficial for the e-NRR while suppressing the competing HER process. Besides N doping, P doping has also been reported to be an effective way to improve the e-NRR activity of carbon matrices.[104,105] For instance, Yuan *et al.* showed that P-doped carbon nanotubes (P-CNTs) delivered ~100 times higher NH_3 yield rate than CNTs.[105] DFT calculations revealed that the adsorption of N_2 was much stronger on P atoms than on the C atom next to the P atom, suggesting that P sites with Lewis acidity should be the catalytic sites for e-NRR. It was further proposed that the e-NRR on P-CNTs followed the distal pathway.

6. Strategies for improving e-NRR efficiency

Currently, the major challenges of current e-NRR are the low NH_3 yield rate and poor selectivity (low faradaic efficiency), which are associated with the catalysts. To improve the performance of an e-NRR catalyst, it is necessary to suppress the competing HER, and simultaneously enhance the intrinsic e-NRR activity. In this section, we will highlight and discuss some effective strategies for improving the e-NRR catalytic activity and selectivity, including vacancy engineering, alloy engineering, hydrophobic engineering and dispersing active sites at the atomic level.

6.1 Vacancy engineering

6.1.1 N-Vacancy. Lv *et al.* recently reported polymeric carbon nitride (PCN) with abundant nitrogen vacancies (NVs) for e-NRR catalysis.[106] The created NVs located at the two-coordinated N (N_{2c}) sites as revealed by the XPS spectra. The electron paramagnetic

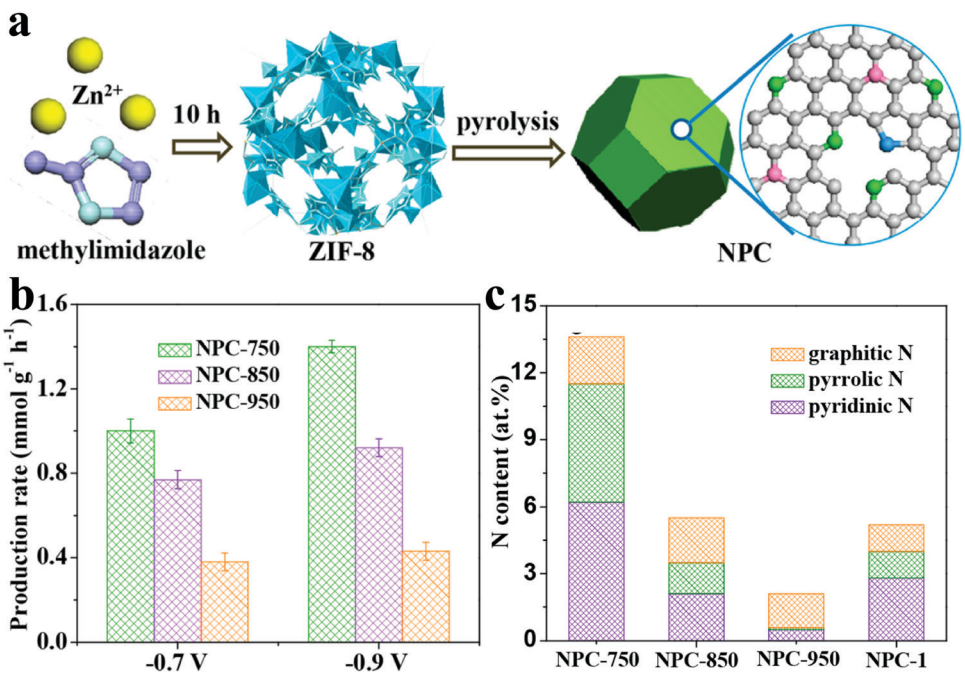

Fig. 9 (a) Schematic illustration of the preparation of NPC. (b) Ammonia production rates of NPC-750, NPC-850, and NPC-950 at −0.7 and −0.9 V. (c) Contents of pyridinic, pyrrolic, and graphitic N in NPCs. Reproduced with permission.[102] Copyright 2018 American Chemistry Society.

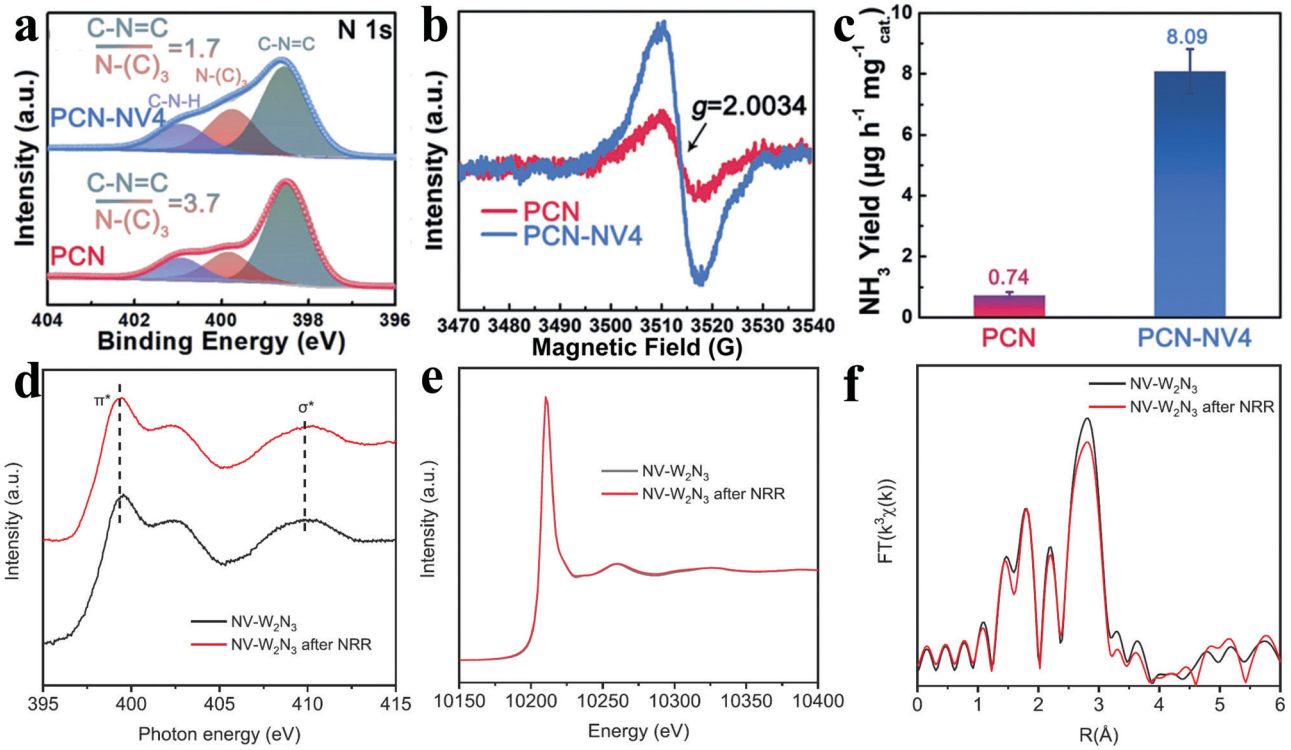

Fig. 10 (a) N 1s XPS spectra. (b) EPR spectra of PCN and PCN-NV4. (c) Yield of ammonia with different catalysts at −0.2 V *versus* RHE. Reproduced with permission from ref. 106 Copyright 2018 Wiley-VCH. (d) Synchrotron-based N K edge XANES spectra. (e) W L3 edge XANES spectra of NV-W_2N_3 before and after NRR test for 10 h. (f) Corresponding FT-EXFAS results of NV-W_2N_3 before and after NRR test for 10 h. Reproduced with permission.[107] Copyright 2019 Wiley-VCH.

resonance (EPR) experiments revealed that the NVs could increase the electron density of their adjacent carbon atoms (Fig. 10a and b). The electrons of the adjacent carbon can further transfer to the adsorbed dinitrogen for activating the N≡N bond and facilitating the reduction of N_2 to NH_3. The PCN with optimized NVs showed a high NH_3 yield rate of 8.09 μg $mg_{cat.}^{-1}$ h^{-1}, which was nearly ten times higher than that of pristine PCN without nitrogen vacancies (Fig. 10c). Jin *et al.* fabricated a 2D layered W_2N_3 nanosheet with surface N vacancies, and applied it to e-NRR catalysis.[107] The 2D W_2N_3 was demonstrated to be e-NRR active with a high NH_3 production rate and faradaic efficiency. DFT calculations showed that N vacancies on the W_2N_3 surface produced an electron deficient area, which can be accommodated by the unpaired electrons of dinitrogen. The adsorbed dinitrogen could be further activated by the electron donation of W to the empty antibonding orbitals of dinitrogen. Furthermore, the N vacancies on 2D W_2N_3 was proven to be stable under e-NRR conditions by the *ex situ* XAS experiments (Fig. 10d–f). In addition, for some metal nitrides, the *in situ* generated N-vacancy could also serve as the active sites following a Mars–van Krevelen mechanism, which was confirmed by the isotope experiments.[25,107–110]

6.1.2 O-Vacancies. Theoretically, oxygen vacancies can generate available localized electrons, which can be donated to the antibonding orbitals of dinitrogen to enable the activation and following hydrogenation of N_2 to NH_3. The introduction of O vacancies can be tuned *via* several methods such as heteroatom dopant,[54,81,83,111,112] thermal reduction,[82,113] and electrochemical polarization.[81] For example, Tong *et al.* prepared Fe-doped $W_{18}O_{49}$ nanowires with abundant oxygen vacancies on carbon fiber paper for efficient e-NRR catalysis.[111] Fe doping increased the oxygen vacancies and simultaneously exposed more active W sites. Theoretical calculations showed that high level oxygen vacancies lead to a shift of $W_{18}O_{49}$ Fermi level toward the π* state of dinitrogen, which was beneficial for the electron back donation from $W_{18}O_{49}$ to dinitrogen for e-NRR. Sun *et al.* reported that the e-NRR activity of WO_3 was positively correlated with the concentration of oxygen vacancies.[113] DFT calculations suggested that the surface oxygen vacancies of WO_3 improved the adsorption of N_2 and lowered the e-NRR thermodynamic barrier. Ding *et al.* also showed that the oxygen vacancies on the Ru-doped CeO_2 surface were beneficial for N_2 adsorption.[54] Nonmetallic dopants such as boron can also promote the generation of O vacancies in transition metal oxides (TMOs). Chu *et al.* reported that replacing the partial O in the MnO_2 lattice with B could readily lead to the formation of oxygen vacancies, which was revealed by the XPS spectra.[112] DFT computations showed that the oxygen vacancies were favorably generated at the B-adjacent sites rather than non-B-adjacent sites. The B dopants and oxygen vacancies synergistically induced asymmetric charge distribution, and thereby improved the catalytic activity of the neighboring Mn sites.

6.2 Alloy engineering

As aforementioned, an alloy engineering strategy is also an effective way to introduce second catalytic sites and/or alter the

electronic structure of catalytic sites, and thereby enhances the e-NRR activity.[40,41,44,47] For example, Jin *et al.* fabricated fusiform-like RuCu alloy nanosheets, which exhibited a much higher NH_3 yield with 53.6 μg^{-1} h^{-1} mg^{-1} and faradaic efficiency of 7.2% than single Ru (15 μg^{-1} h^{-1} mg^{-1} and 1.7%).[47] The enhancement was attributed to the synergistic catalysis of the Ru and Cu sites, which optimized the adsorptive activation of N_2 and desorption of intermediates. Tong *et al.* investigated the e-NRR activity of nanoporous PdCu alloys with different Pd/Cu atom ratios.[44] The average NH_3 yield rates of the electrocatalysts increased in the following order: Pd_3Cu_1 > Pd_6Cu_1 > PdCu > Pd > Cu. The e-NRR activity of Pd_3Cu_1 electrocatalysts is nearly 4.2 and 4.6 times that of the nanoporous Pd and Cu. Hence, the author proposed that the introduced Cu modified the electron structure of Pd and suppressed the competing HER process. Wang *et al.* reported an efficient Pd_3Bi electrocatalyst with a nanoporous ordered intermetallic structure.[114] The operando XAS measurements and DFT calculations indicate that the adsorption and desorption of N species on Bi sites can be modulated by electronic interactions of Pd–Bi compounds. Benefitting from Bi introduced to Pd, the HER process can be effectively suppressed.

6.3 Hydrophobic engineering

Compared with N_2 molecules with extremely low solubility in aqueous electrolyte, the abundant H_3O^+ species in the electrolyte are much more favorable for the mass transfer, resulting in the high coverage of catalytic sites by H^+. An effective strategy to alleviate H^+ migrating to the surface of the catalyst is the surface hydrophobic modification of substrates or electrocatalysts. Yu *et al.* fabricated a thin hydrophobic carbon layer on the SnS nanosheets surface to enhance its e-NRR activity.[115] The hydrophobic carbon layer served as a protective shield to limit the proton availability at the SnS surface and simultaneously enhance the N_2 adsorption and conductivity, thus greatly boosted the e-NRR activity of SnS. In addition, a hydrophobic zeolitic imidazole framework (ZIF) was also employed to regulate water availability towards the electrocatalyst surface.[116–118] For example, Yang *et al.* reported that ZIF-8 coated nanoporous gold exhibited excellent e-NRR catalytic activity with a NH_3 yield rate of 28.7 $\mu g\ h^{-1}\ cm^{-2}$ and a faradaic efficiency of 44% (Fig. 11). The hydrophobic porous ZIF-8 shell on nanoporous gold was demonstrated to be significant for suppressing hydrogen evolution by hindering the diffusion of reactants.[118] However, we speculate that the ZIF-8 structure cannot survive under the harsh electrochemical condition.[119]

6.4 Single-atom catalysts

Single-atom catalysts (SACs), a class of materials with atomically distributed active sites, have emerged as a hot research field in the catalytic community due to their maximum atomic efficiency and unique catalytic ability.[120] In recent years, many highly dispersed single atoms such as Ni,[121] Fe,[122–124] Mo,[65] Cu,[125] Ru,[49,50] and Co,[126] have been applied for desirable electrocatalytic reactions for nitrogen fixation. The electronic structures of single-atom active centers can be effectively tuned by the surrounding coordination atoms. For example, the Fe–N_4 species in Fe-SAC/NC, which was quantitatively analyzed by the EXAFS fitting, was demonstrated to be responsible for the excellent e-NRR performance of Fe-SAC/NC (Fig. 12).[124] It was shown that the Fe 3d electrons were transferred to the N 2p, resulting in the activation of dinitrogen for the subsequent hydrogenation. Besides Fe–N_4, Fe–N_3 species and Cu–N_2 species in Cu SAC/NC were also found to be able to enhance the e-NRR activity.[122,125] Recently, it was reported that Fe–MoS_2 with protrusion-shaped Fe single atoms exhibited strong interfacial polarization, thus efficiently activated N≡N triple bonds to boost electrocatalytic NH_3 synthesis.[127] Liu *et al.* employed DFT calculations to systematically study the e-NRR activity of dozens of SACs. They predicted that Ru and Rh single atoms supported on g-C_3N_4 are the most promising electrocatalysts for the e-NRR.[128]

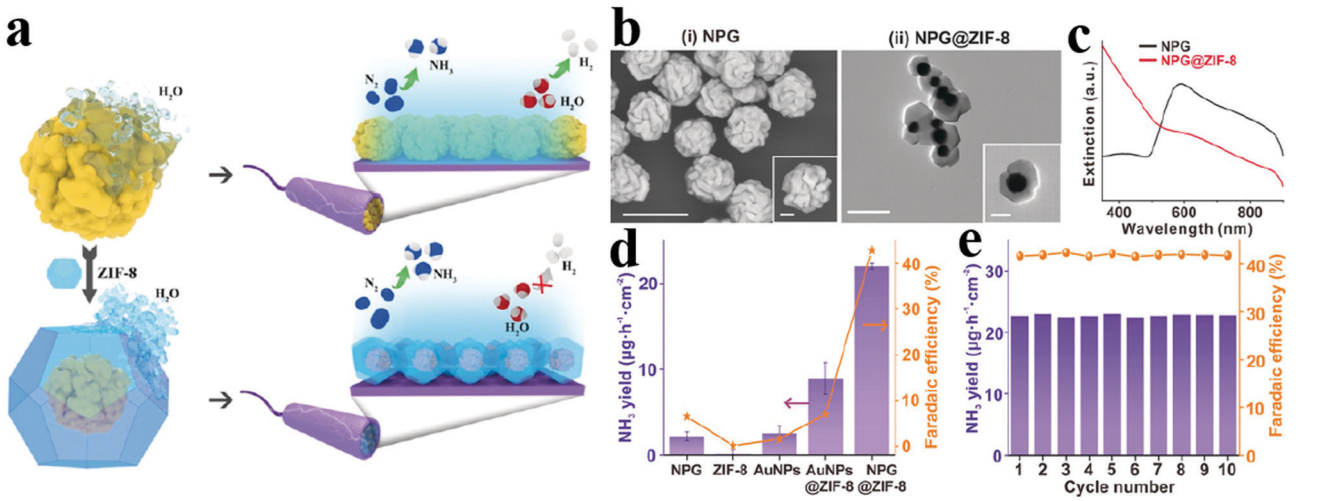

Fig. 11 (a) Schematic depiction of nitrogen reduction enhancement by NPG@ZIF-8 electrocatalyst, (b) (i) SEM image of NPG cores and scale bar: 500 nm (inset: 100 nm); (ii) TEM image of NPG@ZIF-8 composite and scale bar: 1 μm (inset: 300 nm), (c) corresponding UV-vis absorption spectra, (d) comparison of catalytic performances of various electrocatalysts, and (e) cycling tests of a NPG@ZIF-8 catalyst at −0.6 V *vs.* RHE. Reproduced with permission.[118] Copyright 2019 Wiley-VCH.

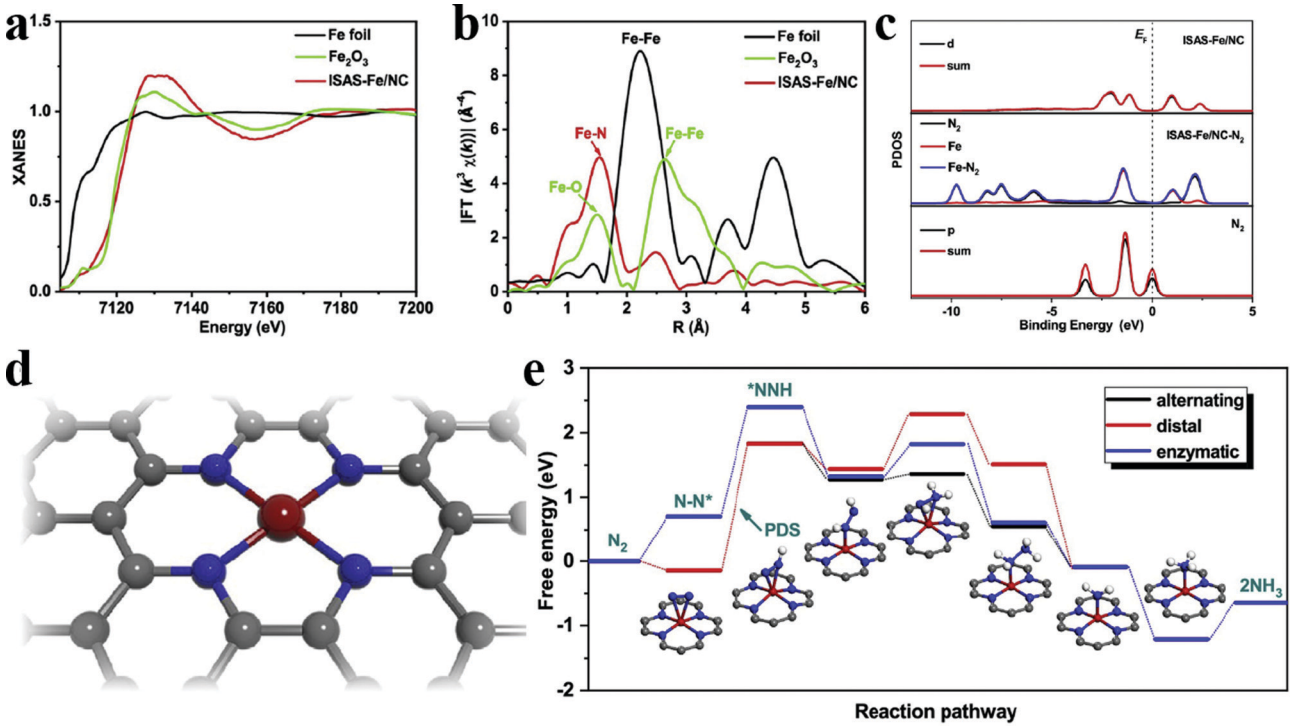

Fig. 12 (a and b) Synchrotron radiation XANES measurements of (a) XANES and (b) FT-EXAFS curves of ISAS-Fe/NC at Fe K-edge, (c) PDOS for ISAS-Fe/NC, ISAS-Fe/NC-N_2 and N_2 configurations (the Fermi level is set at 0 eV), (d) schematic model of ISAS-Fe/NC, and (e) free energy profiles for NRR on ISAS-e/NC with three possible pathways. Reproduced with permission.[124] Copyright 2019 Elsevier.

7. Perspectives

Electrochemical nitrogen fixation under mild conditions is one sustainable alternative to the traditional Haber–Bosch process. In this review, we have briefly summarized recent efforts devoted to developing electrocatalysts, including noble-metal based materials, transition-metal based materials, and metal-free materials, for e-NRR catalysis. In addition, strategies such as vacancy engineering, and hydrophobic engineering have been proposed to boost e-NRR by enhancing N_2 adsorption ability and hindering the competing HER process. To develop e-NRR catalysts applicable for practical application, substantial further efforts are still required. To accelerate the development, we need to understand the fundamental mechanism of e-NRR at an atomistic level by using a combination of theoretical calculations and *in situ* experimental characterizations. Theoretical calculation is a powerful tool to investigate e-NRR reactions on an electrocatalyst surface at an atomistic level. Various e-NRR mechanisms have been predicted based on the theoretical calculations. However, the computational methods usually overlooked the influence of electrolyte molecules and/or ions. The calculation results are pH-independent, and are not usually consistent with the experimental findings. Therefore, it is highly necessary to reveal the e-NRR intermediates and structural transformations of electrocatalyst by means of *in situ* experimental techniques, such as *in situ* XPS, *in situ* TEM and *in situ* XAS. In addition, some electrolytes or cations are found to be beneficial for the e-NRR catalysis. For example, lithium-mediated aqueous solutions are able to activate N_2 and suppress the HER process.[129] K^+ cations in the electrolyte can be easily adsorbed on the surface of Bi nanoplates, and thereby modify the surface electronic structures of Bi to enhance the yield and selectivity of ammonia. Therefore, further research efforts should be also focused on understanding the influence of electrolytes on e-NRR catalysis. Furthermore, modulating the mass transfer at the interface of catalysts is another effective strategy to promote e-NRR. For example, exfoliated covalent organic frameworks (ECOF) prepared by Yan and coworkers can decrease the accessibility of H^+ to the surface of boron-doped carbon paper (BCP) and promote the molecular collisions between N_2 molecules and BCP.[130]

8. Challenges

It is worthwhile that current electrochemical N_2 fixation still faces a grand challenge for its low ammonia yield rate. The majority of investigated materials exhibit more negative onset potentials for e-NRR than those for HER. The highest ammonia yield rates reported in the literature are only several dozens of micrograms per hour per square centimeter of electrode (or per milligram of catalyst), which is obviously far below the requirement for practical applications. On the other hand, due to the low ammonia yield rate of catalysts, the influence of ambient ammonia contamination on the results could be significant, which make it very difficult to accurately measure the e-NRR-generated NH_3. It has been reported that the ammonia contaminations can be from various sources, such as the atmosphere

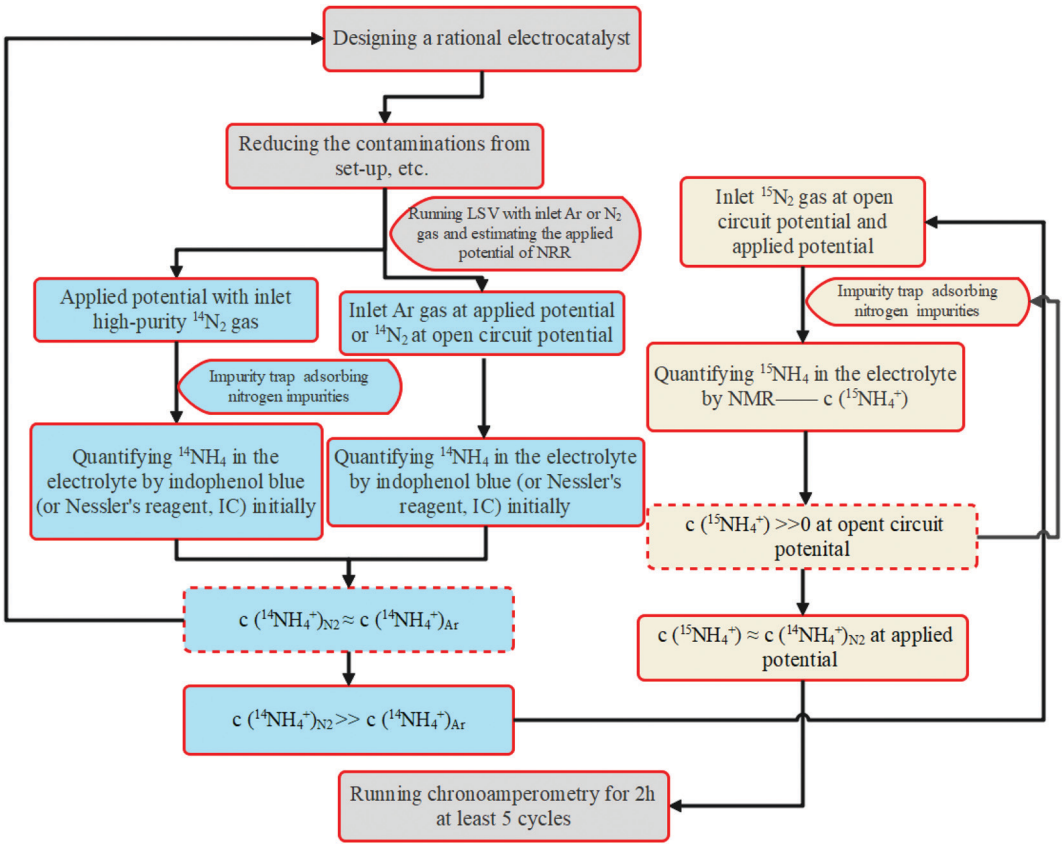

Fig. 13 The flow program of the suggested protocols for rigorous experimental measurements.

(~10 μg m^{-3}), human respiration, reaction setups, nitrogen-containing chemicals, and impurity of N_2 supply.[131,132] In particular, even the highly pure N_2 may contain NH_3 and easily reduced NO_x specie.[133] For example, a highly pure N_2 with only 0.006% of NO, can readily lead to the formation of NH_3 under electroreduction conditions with a yield rate of 26.3 μg cm^{-2} h^{-1}.[134] Moreover, the decomposition of nitrogen-containing catalysts also causes a false positive result.[135] Recently, Andersen *et al.* attempted to reproduce the e-NRR activities of the most promising materials reported in the literature *via* a rigorous experimental procedure using $^{15}N_2$. However, the results showed that the majority of them are not reproducible. Therefore, it is necessary to establish a testing procedure for reliable ammonia measurements. In e-NRR experiments, spectrophotometric methods including an indophenol blue method and Nessler's reagent are widely used for the detection of ammonia. However, indophenol blue assay is not accurate when the NH_3 concentration is up to 500 μg L^{-1}. Compared with indophenol blue, Nessler's reagent is favorably used under both acidic and alkaline media.[136] Ion chromatography is capable of quantifying extremely tiny amounts of ammonia with a low detection limit of 1 μg L^{-1}.[137] Therefore, to ensure accurate quantification of ammonia, a combined spectrophotometric and IC measurement is suggested. Moreover, to confirm the origin of ammonia, ^{15}N isotopic labeling experiments should be performed. Herein, we presented a rigorous e-NRR experimental procedure as shown in Fig. 13. Although the accurate detection using the rigorous experimental measurement is highly required for the current electrocatalysts reported, it is not the case for an e-NRR electrocatalyst with desirable ammonia yield, which is several orders of magnitude higher than the possible contamination.

Conflicts of interest

There are no conflicts to declare.

Acknowledgements

This work was supported by the "From 0 to 1" Innovative program of CAS (No. ZDBS-LY-JSC021), the National Natural Science Foundation (No. 51872306), the Natural Science Foundation of Zhejiang Province (No. D21E020002 and LY21E020008), the Youth Innovation Promotion Association of the Chinese Academy of Sciences (No. 2020300), the "Science and Technology Innovation 2025" major programs in Ningbo (2019B10046 and 2019B10041) and the K. C. Wong Education Foundation (GJTD-2019-13).

References

1 N. Gruber and J. N. Galloway, An earth-system perspective of the global nitrogen cycle, *Nature*, 2008, **451**, 293–296.
2 V. Smil, Detonator of the population explosion, *Nature*, 1999, **400**, 415.

3 R. Schlogl, Catalytic synthesis of ammonia-a ''never-ending story''?, *Angew. Chem., Int. Ed.*, 2003, **42**, 2004–2008.
4 F. Ishak, I. Dincer and C. Zamfirescu, Thermodynamic analysis of ammonia-fed solid oxide fuel cells, *J. Power Sources*, 2012, **202**, 157–165.
5 C. Tang and S. Z. Qiao, How to explore ambient electrocatalytic nitrogen reduction reliably and insightfully, *Chem. Soc. Rev.*, 2019, **48**, 3166–3180.
6 T. Xu, B. Ma, J. Liang, L. Yue, Q. Liu, T. Li, H. Zhao, Y. Luo, S. Lu and X. Sun, Recent Progress in Metal-Free Electrocatalysts toward Ambient N2 Reduction Reaction, *Acta Phys.-Chim. Sin.*, 2020, 2009043.
7 L. Wang, M. K. Xia, H. Wang, K. F. Huang, C. X. Qian, C. T. Maravelias and G. A. Ozin, Greening ammonia toward the solar ammonia refinery, *Joule*, 2018, **2**, 1055–1074.
8 C. J. M. van der Ham, M. T. M. Koper and D. G. H. Hetterscheid, Challenges in reduction of dinitrogen by proton and electron transfer, *Chem. Soc. Rev.*, 2014, **43**, 5183–5191.
9 B. Ma, H. Zhao, T. Li, Q. Liu, Y. Luo, C. Li, S. Lu, A. M. Asiri, D. Ma and X. Sun, Iron-group electrocatalysts for ambient nitrogen reduction reaction in aqueous media, *Nano Res.*, 2021, **14**, 555–569.
10 J. Kim and D. C. Rees, Nitrogenase and biological nitrogen fixation, *Biochemistry*, 1994, **33**, 389–397.
11 J. S. Anderson, J. Rittle and J. C. Peters, Catalytic conversion of nitrogen to ammonia by an iron model complex, *Nature*, 2013, **501**, 84–87.
12 J. Gao, X. Lv, F. Wang, Y. Luo, S. Lu, G. Chen, S. Gao, B. Zhong, X. Guo and X. Sun, Enabling electrochemical conversion of N2 to NH3 under ambient conditions by a CoP3 nanoneedle array, *J. Mater. Chem. A*, 2020, **8**, 17956–17959.
13 P. Wei, Q. Geng, A. I. Channa, X. Tong, Y. Luo, S. Lu, G. Chen, S. Gao, Z. Wang and X. Sun, Electrocatalytic N2 reduction to NH3 with high faradaic efficiency enabled by vanadium phosphide nanoparticle on V foil, *Nano Res.*, 2020, **13**, 2967–2972.
14 R. Zhao, Q. Geng, L. Chang, P. Wei, Y. Luo, X. Shi, A. M. Asiri, S. Lu, Z. Wang and X. Sun, Cu3P nanoparticle-reduced graphene oxide hybrid: an efficient electrocatalyst to realize N2-to-NH3 conversion under ambient conditions, *Chem. Commun.*, 2020, **56**, 9328–9331.
15 T. Wang, S. Li, B. He, X. Zhu, Y. Luo, Q. Liu, T. Li, S. Lu, C. Ye, A. M. Asiri and X. Sun, Commercial indium-tin oxide glass: A catalyst electrode for efficient N2 reduction at ambient conditions, *Chin. J. Catal.*, 2021, **42**, 1024–1029.
16 S. Li, Y. Wang, J. Liang, T. Xu, D. Ma, Q. Liu, T. Li, S. Xu, G. Chen, A. M. Asiri, Y. Luo, Q. Wu and X. Sun, TiB2 thin film enabled efficient NH3 electrosynthesis at ambient conditions, *Mater. Today Phys.*, 2021, **18**, 100396.
17 T. Xu, J. Liang, S. Li, Z. Xu, L. Yue, T. Li, Y. Luo, Q. Liu, X. Shi, A. M. Asiri, C. Yang and X. Sun, Recent Advances in Nonprecious Metal Oxide Electrocatalysts and Photocatalysts for N2 Reduction Reaction under Ambient Condition, *Small Sci.*, 2021, **1**, 2000069.
18 X. Guo, H. Du, F. Qu and J. Li, Recent progress in electrocatalytic nitrogen reduction, *J. Mater. Chem. A*, 2019, **7**, 3531–3543.
19 C. J. van der Ham, M. T. Koper and D. G. Hetterscheid, Challenges in reduction of dinitrogen by proton and electron transfer, *Chem. Soc. Rev.*, 2014, **43**, 5183–5191.
20 E. Skulason, T. Bligaard, S. Gudmundsdottir, F. Studt, J. Rossmeisl, F. Abild-Pedersen, T. Vegge, H. Jonsson and J. K. Norskov, A theoretical evaluation of possible transition metal electro-catalysts for N2 reduction, *Phys. Chem. Chem. Phys.*, 2012, **14**, 1235–1245.
21 Y. Yao, S. Zhu, H. Wang, H. Li and M. Shao, A spectroscopic study on the nitrogen electrochemical reduction reaction on gold and Platinum surfaces, *J. Am. Chem. Soc.*, 2018, **140**, 1496–1501.
22 Y. Yao, S. Zhu, H. Wang, H. Li and M. Shao, A spectroscopic study of electrochemical nitrogen and nitrate reduction on Rhodium surfaces, *Angew. Chem., Int. Ed.*, 2020, **59**, 10479–10483.
23 D. Yao, C. Tang, L. Li, B. Xia, A. Vasileff, H. Jin, Y. Zhang and S. Z. Qiao, In situ fragmented bismuth nanoparticles for electrocatalytic nitrogen reduction, *Adv. Energy Mater.*, 2020, **10**, 2001289.
24 Y. Abghoui, A. L. Garden, J. G. Howalt, T. Vegge and E. Skúlason, Electroreduction of N2 to ammonia at ambient conditions on mononitrides of Zr, Nb, Cr, and V: A DFT guide for experiments, *ACS Catal.*, 2016, **6**, 635–646.
25 Y. Abghoui and E. Skúlason, Electrochemical synthesis of ammonia via Mars-van Krevelen mechanism on the (111) facets of group III–VII transition metal mononitrides, *Catal. Today*, 2017, **286**, 78–84.
26 X.-F. Li, Q.-K. Li, J. Cheng, L. Liu, Q. Yan, Y. Wu, X.-H. Zhang, Z.-Y. Wang, Q. Qiu and Y. Luo, Conversion of dinitrogen to ammonia by FeN3-embedded graphene, *J. Am. Chem. Soc.*, 2016, **138**, 8706–8709.
27 D. Bao, Q. Zhang, F. L. Meng, H. X. Zhong, M. M. Shi, Y. Zhang, J. M. Yan, Q. Jiang and X. B. Zhang, Electrochemical reduction of N2 under ambient conditions for artificial N2 fixation and renewable energy storage using N2/NH3 cycle, *Adv. Mater.*, 2017, **29**, 1604799.
28 M. M. Shi, D. Bao, B. R. Wulan, Y. H. Li, Y. F. Zhang, J. M. Yan and Q. Jiang, Au sub-nanoclusters on TiO2 toward highly efficient and selective electrocatalyst for N2 conversion to NH3 at ambient conditions, *Adv. Mater.*, 2017, **29**, 1606550.
29 L. Tan, N. Yang, X. Huang, L. Peng, C. Tong, M. Deng, X. Tang, L. Li, Q. Liao and Z. Wei, Synthesis of ammonia via electrochemical nitrogen reduction on high-index faceted Au nanoparticles with a high faradaic efficiency, *Chem. Commun.*, 2019, **55**, 14482–14485.
30 J. Zheng, Y. Lyu, M. Qiao, J. P. Veder, R. D. Marco, J. Bradley, R. Wang, Y. Li, A. Huang, S. P. Jiang and S. Wang, Tuning the electron localization of gold enables the control of nitrogen-to-ammonia fixation, *Angew. Chem., Int. Ed.*, 2019, **58**, 18604–18609.
31 D. Liu, G. Zhang, Q. Ji, Y. Zhang and J. Li, Synergistic electrocatalytic nitrogen reduction enabled by confinement of nanosized Au particles onto a two-dimensional Ti3C2 substrate, *ACS Appl. Mater. Interfaces*, 2019, **11**, 25758–25765.

32 J. Zhang, Y. Ji, P. Wang, Q. Shao, Y. Li and X. Huang, Adsorbing and activating N2 on heterogeneous Au–Fe3O4 nanoparticles for N2 fixation, *Adv. Funct. Mater.*, 2019, **30**, 1906579.

33 Y. Zhou, X. Yu, X. Wang, C. Chen, S. Wang and J. Zhang, MoS2 nanosheets supported gold nanoparticles for electrochemical nitrogen fixation at various pH value, *Electrochim. Acta*, 2019, **317**, 34–41.

34 S. Zhao, H.-X. Liu, Y. Qiu, S.-Q. Liu, J.-X. Diao, C.-R. Chang, R. Si and X.-H. Guo, An oxygen vacancy-rich two-dimensional Au/TiO2 hybrid for synergistically enhanced electrochemical N2 activation and reduction, *J. Mater. Chem. A*, 2020, **8**, 6586–6596.

35 P. Wang, Y. Ji, Q. Shao, Y. Li and X. Huang, Core@shell structured Au@SnO_2 nanoparticles with improved N2 adsorption/activation and electrical conductivity for efficient N2 fixation, *Sci. Bull.*, 2020, **65**, 350–358.

36 M. Nazemi, S. R. Panikkanvalappil and M. A. El-Sayed, Enhancing the rate of electrochemical nitrogen reduction reaction for ammonia synthesis under ambient conditions using hollow gold nanocages, *Nano Energy*, 2018, **49**, 316–323.

37 J. Wang, L. Yu, L. Hu, G. Chen, H. Xin and X. Feng, Ambient ammonia synthesis via palladium-catalyzed electrohydrogenation of dinitrogen at low overpotential, *Nat. Commun.*, 2018, **9**, 1795.

38 G. Deng, T. Wang, A. A. Alshehri, K. A. Alzahrani, Y. Wang, H. Ye, Y. Luo and X. Sun, Improving the electrocatalytic N2 reduction activity of Pd nanoparticles through surface modification, *J. Mater. Chem. A*, 2019, **7**, 21674–21677.

39 H. Zhao, D. Zhang, H. Li, W. Qi, X. Wu, Y. Han, W. Cai, Z. Wang, J. Lai and L. Wang, Exposure of definite palladium facets boosts electrocatalytic nitrogen fixation at low overpotential, *Adv. Energy Mater.*, 2020, **10**, 2002131.

40 F. Pang, Z. Wang, K. Zhang, J. He, W. Zhang, C. Guo and Y. Ding, Bimodal nanoporous Pd3Cu1 alloy with restrained hydrogen evolution for stable and high yield electrochemical nitrogen reduction, *Nano Energy*, 2019, **58**, 834–841.

41 F. Pang, F. Wang, L. Yang, Z. Wang and W. Zhang, Hierarchical nanoporous Pd1Ag1 alloy enables efficient electrocatalytic nitrogen reduction under ambient conditions, *Chem. Commun.*, 2019, **55**, 10108–10111.

42 H. Zhao, D. Zhang, Z. Wang, Y. Han, X. Sun, H. Li, X. Wu, Y. Pan, Y. Qin, S. Lin, Z. Xu, J. Lai and L. Wang, High-performance nitrogen electroreduction at low overpotential by introducing Pb to Pd nanosponges, *Appl. Catal., B*, 2020, **265**, 118481.

43 M. Ma, X. Han, H. Li, X. Zhang, Z. Zheng, L. Zhou, J. Zheng, Z. Xie, Q. Kuang and L. Zheng, Tuning electronic structure of PdZn nanocatalyst via acid-etching strategy for highly selective and stable electrolytic nitrogen fixation under ambient conditions, *Appl. Catal., B*, 2020, **265**, 118568.

44 W. Tong, B. Huang, P. Wang, L. Li, Q. Shao and X. Huang, Crystal-phase-engineered PdCu electrocatalyst for enhanced ammonia synthesis, *Angew. Chem., Int. Ed.*, 2020, **59**, 2649–2653.

45 W. Xu, G. Fan, J. Chen, J. Li, L. Zhang, S. Zhu, X. Su, F. Cheng and J. Chen, Nanoporous palladium hydride for electrocatalytic N2 reduction under ambient conditions, *Angew. Chem., Int. Ed.*, 2020, **59**, 3511–3516.

46 Y. Yao, H. Wang, X.-Z. Yuan, H. Li and M. Shao, Electrochemical nitrogen reduction reaction on ruthenium, *ACS Energy Lett.*, 2019, **4**, 1336–1341.

47 Y. Jin, X. Ding, L. Zhang, M. Cong, F. Xu, Y. Wei, S. Hao and Y. Gao, Boosting electrocatalytic reduction of nitrogen to ammonia under ambient conditions by alloy engineering, *Chem. Commun.*, 2020, **56**, 11477–11480.

48 W. Peng, M. Luo, X. Xu, K. Jiang, M. Peng, D. Chen, T. S. Chan and Y. Tan, Spontaneous atomic Ruthenium doping in Mo2CTX MXene defects enhances electrocatalytic activity for the nitrogen reductio reaction, *Adv. Energy Mater.*, 2020, **10**, 2001364.

49 H. Tao, C. Choi, L.-X. Ding, Z. Jiang, Z. Han, M. Jia, Q. Fan, Y. Gao, H. Wang, A. W. Robertson, S. Hong, Y. Jung, S. Liu and Z. Sun, Nitrogen fixation by Ru single-atom electrocatalytic reduction, *Chem*, 2019, **5**, 204–214.

50 Z. Geng, Y. Liu, X. Kong, P. Li, K. Li, Z. Liu, J. Du, M. Shu, R. Si and J. Zeng, Achieving a record-high yield rate of 120.9 mug NH3 mgcat.-1 h-1 for N2 electrochemical reduction over Ru single-atom catalysts, *Adv. Mater.*, 2018, **30**, 1803498.

51 Z. Wang, C. Li, K. Deng, Y. Xu, H. Xue, X. Li, L. Wang and H. Wang, Ambient nitrogen reduction to ammonia electrocatalyzed by bimetallic PdRu porous nanostructures, *ACS Sustainable Chem. Eng.*, 2018, **7**, 2400–2405.

52 L. Zhao, J. Zhao, J. Zhao, L. Zhang, D. Wu, H. Wang, J. Li, X. Ren and Q. Wei, Artificial N2 fixation to NH3 by electrocatalytic Ru NPs at low overpotential, *Nanotechnology*, 2020, **31**, 29LT01.

53 H. Wang, Y. Li, D. Yang, X. Qian, Z. Wang, Y. Xu, X. Li, H. Xue and L. Wang, Direct fabrication of bi-metallic PdRu nanorod assemblies for electrochemical ammonia synthesis, *Nanoscale*, 2019, **11**, 5499–5505.

54 Y. Ding, L. Huang, J. Zhang, A. Guan, Q. Wang, L. Qian, L. Zhang and G. Zheng, Ru-doped, oxygen-vacancy-containing CeO2 nanorods toward N2 electroreduction, *J. Mater. Chem. A*, 2020, **8**, 7229–7234.

55 S. Back and Y. Jung, On the mechanism of electrochemical ammonia synthesis on the Ru catalyst, *Phys. Chem. Chem. Phys.*, 2016, **18**, 9161–9166.

56 A. Liu, M. Gao, X. Ren, F. Meng, Y. Yang, Q. Yang, W. Guan, L. Gao, X. Liang and T. Ma, A two-dimensional Ru@MXene catalyst for highly selective ambient electrocatalytic nitrogen reduction, *Nanoscale*, 2020, **12**, 10933–10938.

57 D. V. Yandulov and R. R. Schrock, Catalytic reduction of dinitrogen to ammonia at a single molybdenum center, *Science*, 2003, **301**, 76.

58 H. Cheng, L. X. Ding, G. F. Chen, L. Zhang, J. Xue and H. Wang, Molybdenum carbide nanodots enable efficient electrocatalytic nitrogen fixation under ambient conditions, *Adv. Mater.*, 2018, **30**, 1803694.

59 L. Zhang, X. Ji, X. Ren, Y. Ma, X. Shi, Z. Tian, A. M. Asiri, L. Chen, B. Tang and X. Sun, Electrochemical ammonia

synthesis via nitrogen reduction reaction on a MoS_2 catalyst: Theoretical and experimental studies, *Adv. Mater.*, 2018, **30**, 1800191.

60 J. Chen, C. Zhang, M. Huang, J. Zhang, J. Zhang, H. Liu, G. Wang and R. Wang, The activation of porous atomic layered MoS2 basal-plane to induce adjacent Mo atom pairs promoting high efficiency electrochemical N2 fixation, *Appl. Catal., B*, 2021, **285**, 119810.

61 X. Xu, B. Sun, Z. Liang, H. Cui and J. Tian, High-performance electrocatalytic conversion of N2 to NH3 using 1T-MoS2 anchored on Ti3C2 MXene under ambient conditions, *ACS Appl. Mater. Interfaces*, 2020, **12**, 26060–26067.

62 L. Yang, H. Wang, X. Wang, W. Luo, C. Wu, C. A. Wang and C. Xu, Flower-like hollow MoSe2 nanospheres as efficient earth-abundant electrocatalysts for nitrogen reduction reaction under ambient conditions, *Inorg. Chem.*, 2020, **59**, 12941–12946.

63 T. Wang, Q. Liu, T. Li, S. Lu, G. Chen, X. Shi, A. M. Asiri, Y. Luo, D. Ma and X. Sun, A magnetron sputtered Mo3Si thin film: an efficient electrocatalyst for N2 reduction under ambient conditions, *J. Mater. Chem. A*, 2021, **9**, 884–888.

64 X. Qu, L. Shen, Y. Mao, J. Lin, Y. Li, G. Li, Y. Zhang, Y. Jiang and S. Sun, Facile preparation of carbon shells-coated O-doped molybdenum carbide nanoparticles as high selective electrocatalysts for nitrogen reduction reaction under ambient conditions, *ACS Appl. Mater. Interfaces*, 2019, **11**, 31869–31877.

65 L. Han, X. Liu, J. Chen, R. Lin, H. Liu, F. Lu, S. Bak, Z. Liang, S. Zhao, E. Stavitski, J. Luo, R. R. Adzic and H. L. Xin, Atomically dispersed molybdenum catalysts for efficient ambient nitrogen fixation, *Angew. Chem., Int. Ed.*, 2019, **58**, 2321–2325.

66 Y. Ma, T. Yang, H. Zou, W. Zang, Z. Kou, L. Mao, Y. Feng, L. Shen, S. J. Pennycook, L. Duan, X. Li and J. Wang, Synergizing Mo single atoms and Mo2C nanoparticles on CNTs synchronizes selectivity and activity of electrocatalytic N2 reduction to ammonia, *Adv. Mater.*, 2020, **32**, 2002177.

67 N. Han, P. Ding, L. He, Y. Li and Y. Li, Promises of main group metal–based nanostructured materials for electrochemical CO_2 reduction to formate, *Adv. Energy Mater.*, 2019, **10**, 1902338.

68 J. Greeley, T. F. Jaramillo, J. Bonde, I. B. Chorkendorff and J. K. Norskov, Computational high-throughput screening of electrocatalytic materials for hydrogen evolution, *Nat. Mater.*, 2006, **5**, 909–913.

69 Y.-C. Hao, Y. Guo, L.-W. Chen, M. Shu, X.-Y. Wang, T.-A. Bu, W.-Y. Gao, N. Zhang, X. Su, X. Feng, J.-W. Zhou, B. Wang, C.-W. Hu, A.-X. Yin, R. Si, Y.-W. Zhang and C.-H. Yan, Promoting nitrogen electroreduction to ammonia with bismuth nanocrystals and potassium cations in water, *Nat. Catal.*, 2019, **2**, 448–456.

70 L. Li, C. Tang, B. Xia, H. Jin, Y. Zheng and S.-Z. Qiao, Two-dimensional mosaic bismuth nanosheets for highly selective ambient electrocatalytic nitrogen reduction, *ACS Catal.*, 2019, **9**, 2902–2908.

71 L. Xia, W. Fu, P. Zhuang, Y. Cao, M. O. L. Chee, P. Dong, M. Ye and J. Shen, Engineering abundant edge sites of bismuth nanosheets toward superior ambient electrocatalytic nitrogen reduction via topotactic transformation, *ACS Sustainable Chem. Eng.*, 2020, **8**, 2735–2741.

72 Y. Qiu, S. Zhao, M. Qin, J. Diao, S. Liu, L. Dai, W. Zhang and X. Guo, Multi-yolk–shell bismuth@porous carbon as a highly efficient electrocatalyst for artificial N2 fixation under ambient conditions, *Inorg. Chem. Front.*, 2020, **7**, 2006–2016.

73 Y. Wang, M. M. Shi, D. Bao, F. L. Meng, Q. Zhang, Y. T. Zhou, K. H. Liu, Y. Zhang, J. Z. Wang, Z. W. Chen, D. P. Liu, Z. Jiang, M. Luo, L. Gu, Q. H. Zhang, X. Z. Cao, Y. Yao, M. H. Shao, Y. Zhang, X. B. Zhang, J. G. Chen, J. M. Yan and Q. Jiang, Generating defect-rich bismuth for enhancing the rate of nitrogen electroreduction to ammonia, *Angew. Chem., Int. Ed.*, 2019, **58**, 9464–9469.

74 Z. Fang, P. Wu, Y. Qian and G. Yu, Gel-derived amorphous BiNi alloy promotes electrocatalytic nitrogen fixation via optimizing nitrogen adsorption and activation, *Angew. Chem., Int. Ed.*, 2020, **2021**, 4275–4281.

75 B. Chang, Q. Liu, N. Chen and Y. Yang, A flower-like bismuth oxide as an efficient, durable and selective slectrocatalyst for artificial N2 fixation in ambient condition, *ChemCatChem*, 2019, **11**, 1884–1888.

76 Y. Sun, Z. Deng, X.-M. Song, H. Li, Z. Huang, Q. Zhao, D. Feng, W. Zhang, Z. Liu and T. Ma, Bismuth-based free-standing electrodes for ambient-condition cmmonia production in neutral media, *Nano-Micro Lett.*, 2020, **12**, 133.

77 R. Zhang, J. Han, B. Zheng, X. Shi, A. M. Asiri and X. Sun, Metal–organic framework-derived shuttle-like V2O3/C for electrocatalytic N2 reduction under ambient conditions, *Inorg. Chem. Front.*, 2019, **6**, 391–395.

78 R. Zhang, H. Guo, L. Yang, Y. Wang, Z. Niu, H. Huang, H. Chen, L. Xia, T. Li, X. Shi, X. Sun, B. Li and Q. Liu, Electrocatalytic N2 fixation over hollow VO2 microspheres at ambient conditions, *ChemElectroChem*, 2019, **6**, 1014–1018.

79 W. Fang, J. Zhao, T. Wu, Y. Huang, L. Yang, C. Liu, Q. Zhang, K. Huang and Q. Yan, Hydrophilic engineering of VOx-based nanosheets for ambient electrochemical ammonia synthesis at neutral pH, *J. Mater. Chem. A*, 2020, **8**, 5913–5918.

80 N. Cao, Z. Chen, K. Zang, J. Xu, J. Zhong, J. Luo, X. Xu and G. Zheng, Doping strain induced bi-Ti(3+) pairs for efficient N2 activation and electrocatalytic fixation, *Nat. Commun.*, 2019, **10**, 2877.

81 L. Yang, T. Wu, R. Zhang, H. Zhou, L. Xia, X. Shi, H. Zheng, Y. Zhang and X. Sun, Insights into defective TiO2 in electrocatalytic N2 reduction: combining theoretical and experimental studies, *Nanoscale*, 2019, **11**, 1555–1562.

82 T. Wu, X. Zhu, Z. Xing, S. Mou, C. Li, Y. Qiao, Q. Liu, Y. Luo, X. Shi, Y. Zhang and X. Sun, Greatly improving electrochemical N2 reduction over TiO2 nanoparticles by iron doping, *Angew. Chem., Int. Ed.*, 2019, **58**, 18449–18453.

83 S. Cheng, Y.-J. Gao, Y.-L. Yan, X. Gao, S.-H. Zhang, G.-L. Zhuang, S.-W. Deng, Z.-Z. Wei, X. Zhong and J.-G. Wang, Oxygen vacancy enhancing mechanism of nitrogen reduction reaction property in Ru/TiO2, *J. Energy Chem.*, 2019, **39**, 144–151.

84 H. Xian, Q. Wang, G. Yu, H. Wang, Y. Li, Y. Wang and T. Li, Electrochemical synthesis of ammonia by zirconia-based catalysts at ambient conditions, *Appl. Catal., A*, 2019, **581**, 116–122.

85 L. Di, X. Chen, Y. T. Liu, J. Yu and B. Ding, Sb2S3 nanoparticles anchored on SnO2 nanofibers: a high-performance hybrid electrocatalyst toward ammonia synthesis under ambient conditions, *Chem. Commun.*, 2019, **55**, 13892–13895.

86 Y. Guo, Y. Cheng, Q. Li and K. Chu, FeTe2 as an earth-abundant metal telluride catalyst for electrocatalytic nitrogen fixation, *J. Energy Chem.*, 2021, **56**, 259–263.

87 H. W. Liu, K. Hu, D. F. Yan, R. Chen, Y. Q. Zou, H. B. Liu and S. Y. Wang, Recent advances on black phosphorus for energy storage, catalysis, and sensor applications, *Adv. Mater.*, 2018, **30**, 1800295.

88 A. Hirsch and F. Hauke, Post-graphene 2D chemistry: The emerging field of molybdenum disulfide and black phosphorus functionalization, *Angew. Chem., Int. Ed.*, 2018, **57**, 4338–4354.

89 Y. T. Liu, D. Li, J. Yu and B. Ding, Stable confinement of black phosphorus quantum dots on black tin oxide nanotubes: A robust, double-active electrocatalyst toward efficient nitrogen fixation, *Angew. Chem., Int. Ed.*, 2019, **58**, 16439–16444.

90 C. Wang, J. Gao, J.-G. Zhao, D.-J. Yan and X.-D. Zhu, Synergistically coupling black phosphorus quantum dots with MnO2 nanosheets for efficient electrochemical nitrogen reduction under ambient conditions, *Small*, 2020, **16**, 1907091.

91 L. Zhang, L. X. Ding, G. F. Chen, X. Yang and H. Wang, Ammonia synthesis under ambient conditions: Selective electroreduction of dinitrogen to ammonia on black phosphorus nanosheets, *Angew. Chem., Int. Ed.*, 2019, **58**, 2612–2616.

92 B. Chang, L. Li, D. Shi, H. Jiang, Z. Ai, S. Wang, Y. Shao, J. Shen, Y. Wu, Y. Li and X. Hao, Metal-free boron carbonitride with tunable boron Lewis acid sites for enhanced nitrogen electroreduction to ammonia, *Appl. Catal., B*, 2021, **283**, 119622.

93 C. Ling, X. Niu, Q. Li, A. Du and J. Wang, Metal-free single atom catalyst for N2 fixation driven by visible light, *J. Am. Chem. Soc.*, 2018, **140**, 14161–14168.

94 Z. Liu, M. Zhang, H. Wang, D. Cang, X. Ji, B. Liu, W. Yang, D. Li and J. Liu, Defective carbon-doped boron nitride nanosheets for highly efficient electrocatalytic conversion of N2 to NH3, *ACS Sustainable Chem. Eng.*, 2020, **8**, 5278–5286.

95 X. Zhang, T. Wu, H. Wang, R. Zhao, H. Chen, T. Wang, P. Wei, Y. Luo, Y. Zhang and X. Sun, Boron nanosheet: An elemental two-dimensional (2D) material for ambient electrocatalytic N2-to-NH3 fixation in neutral media, *ACS Catal.*, 2019, **9**, 4609–4615.

96 D. Zhou, Y. Jia, X. Duan, J. Tang, J. Xu, D. Liu, X. Xiong, J. Zhang, J. Luo, L. Zheng, B. Liu, Y. Kuang, X. Sun and X. Duan, Breaking the symmetry: Gradient in NiFe layered double hydroxide nanoarrays for efficient oxygen evolution, *Nano Energy*, 2019, **60**, 661–666.

97 X. Yu, P. Han, Z. Wei, L. Huang, Z. Gu, S. Peng, J. Ma and G. Zheng, Boron-doped graphene for electrocatalytic N2 reduction, *Joule*, 2018, **2**, 1610–1622.

98 W. Qiu, X. Y. Xie, J. Qiu, W. H. Fang, R. Liang, X. Ren, X. Ji, G. Cui, A. M. Asiri, G. Cui, B. Tang and X. Sun, High-performance artificial nitrogen fixation at ambient conditions using a metal-free electrocatalyst, *Nat. Commun.*, 2018, **9**, 3485.

99 H. Wang, T. Maiyalagan and X. Wang, Review on recent progress in nitrogen-doped graphene: synthesis, characterization, and its potential applications, *ACS Catal.*, 2012, **2**, 781–794.

100 Y. Dong, Q. Zhang, Z. Tian, B. Li, W. Yan, S. Wang, K. Jiang, J. Su, C. W. Oloman, E. L. Gyenge, R. Ge, Z. Lu, X. Ji and L. Chen, Ammonia Thermal Treatment toward Topological Defects in Porous Carbon for Enhanced Carbon Dioxide Electroreduction, *Adv. Mater.*, 2020, **32**, 2001300.

101 S. K. Singh, K. Takeyasu and J. Nakamura, Active sites and mechanism of oxygen reduction reaction electrocatalysis on nitrogen-doped carbon materials, *Adv. Mater.*, 2019, **31**, 1804297.

102 Y. Liu, Y. Su, X. Quan, X. Fan, S. Chen, H. Yu, H. Zhao, Y. Zhang and J. Zhao, Facile ammonia synthesis from electrocatalytic N2 reduction under ambient conditions on N-Doped porous carbon, *ACS Catal.*, 2018, **8**, 1186–1191.

103 C. Chen, D. Yan, Y. Wang, Y. Zhou, Y. Zou, Y. Li and S. Wang, BN pairs enriched defective carbon nanosheets for ammonia synthesis with high efficiency, *Small*, 2019, **15**, 1805029.

104 T. Wu, X. Li, X. Zhu, S. Mou, Y. Luo, X. Shi, A. M. Asiri, Y. Zhang, B. Zheng, H. Zhao and X. Sun, P-Doped graphene toward enhanced electrocatalytic N2 reduction, *Chem. Commun.*, 2020, **56**, 1831–1834.

105 L.-P. Yuan, Z.-Y. Wu, W.-J. Jiang, T. Tang, S. Niu and J.-S. Hu, Phosphorus-doping activates carbon nanotubes for efficient electroreduction of nitrogen to ammonia, *Nano Res.*, 2020, **13**, 1376–1382.

106 C. Lv, Y. Qian, C. Yan, Y. Ding, Y. Liu, G. Chen and G. Yu, Defect engineering metal-free polymeric carbon nitride electrocatalyst for effective nitrogen fixation under ambient conditions, *Angew. Chem., Int. Ed.*, 2018, **57**, 10246–10250.

107 H. Jin, L. Li, X. Liu, C. Tang, W. Xu, S. Chen, L. Song, Y. Zheng and S. Z. Qiao, Nitrogen vacancies on 2D Layered W2N3: A stable and efficient active site for nitrogen reduction reaction, *Adv. Mater.*, 2019, **31**, 1902709.

108 X. Yang, S. Kattel, J. Nash, X. Chang, J. H. Lee, Y. Yan, J. G. Chen and B. Xu, Quantification of active sites and elucidation of the reaction mechanism of the electrochemical nitrogen reduction reaction on vanadium nitride, *Angew. Chem., Int. Ed.*, 2019, **58**, 13768–13772.

109 J. Nash, X. Yang, J. Anibal, M. Dunwell, S. Yao, K. Attenkofer, J. G. Chen, Y. Yan and B. Xu, Elucidation of the active phase and deactivation mechanisms of chromium nitride in the electrochemical nitrogen reduction reaction, *J. Phys. Chem. C*, 2019, **123**, 23967–23975.

110 N. Yu, W. Cao, M. Huttula, Y. Kayser, P. Hoenicke, B. Beckhoff, F. Lai, R. Dong, H. Sun and B. Geng, Fabrication of FeNi hydroxides double-shell nanotube arrays with enhanced performance for oxygen evolution reaction, *Appl. Catal., B*, 2020, **261**, 118193.

111 Y. Tong, H. Guo, D. Liu, X. Yan, P. Su, J. Liang, S. Zhou, J. Liu, G. Q. M. Lu and S. X. Dou, Vacancy engineering of iron-doped W18O49 nanoreactors for low-barrier electrochemical nitrogen reduction, *Angew. Chem., Int. Ed.*, 2020, **59**, 7356–7361.

112 K. Chu, Y.-P. Liu, Y.-H. Cheng and Q.-Q. Li, Synergistic boron-dopants and boron-induced oxygen vacancies in MnO2 nanosheets to promote electrocatalytic nitrogen reduction, *J. Mater. Chem. A*, 2020, **8**, 5200–5208.

113 Z. Sun, R. Huo, C. Choi, S. Hong, T.-S. Wu, J. Qiu, C. Yan, Z. Han, Y. Liu, Y.-L. Soo and Y. Jung, Oxygen vacancy enables electrochemical N2 fixation over WO3 with tailored structure, *Nano Energy*, 2019, **62**, 869–875.

114 X. Wang, M. Luo, J. Lan, M. Peng and Y. Tan, Nanoporous Intermetallic Pd3Bi for Efficient Electrochemical Nitrogen Reduction, *Adv. Mater.*, 2021, e2007733.

115 W. Yu, F. Shu, Y. Huang, F. Yang, Q. Meng, Z. Zou, J. Wang, Z. Zeng, G. Zou and S. Deng, Enhanced electrocatalytic nitrogen reduction activity by incorporation of a carbon layer on SnS microflowers, *J. Mater. Chem. A*, 2020, **8**, 20677–20686.

116 H. Y. F. Sim, J. R. T. Chen, C. S. L. Koh, H. K. Lee, X. Han, G. C. Phan-Quang, J. Y. Pang, C. L. Lay, S. Pedireddy, I. Y. Phang, E. K. L. Yeow and X. Y. Ling, ZIF-induced d-band modification in a bimetallic nanocatalyst: Achieving over 44% efficiency in the ambient nitrogen reduction reaction, *Angew. Chem., Int. Ed.*, 2020, **59**, 16997–17003.

117 C. S. L. Koh, H. K. Lee, H. Y. Fan Sim, X. Han, G. C. Phan-Quang and X. Y. Ling, Turning water from a hindrance to the promotor of preferential electrochemical nitrogen reduction, *Chem. Mater.*, 2020, **32**, 1674–1683.

118 Y. Yang, S. Q. Wang, H. Wen, T. Ye, J. Chen, C. P. Li and M. Du, Nanoporous gold embedded ZIF composite for enhanced electrochemical nitrogen fixation, *Angew. Chem., Int. Ed.*, 2019, **58**, 15362–15366.

119 Y. C. Lin, C. L. Kong, Q. J. Zhang and L. Chen, Metal-organic frameworks for carbon dioxide capture and methane storage, *Adv. Energy Mater.*, 2017, **7**, 1601296.

120 Y. Lin, P. Liu, E. Velasco, G. Yao, Z. Tian, L. Zhang and L. Chen, Fabricating single-atom catalysts from chelating metal in open frameworks, *Adv. Mater.*, 2019, **31**, 1808193.

121 S. Mukherjee, X. Yang, W. Shan, W. Samarakoon, S. Karakalos, D. A. Cullen, K. More, M. Wang, Z. Feng, G. Wang and G. Wu, Atomically dispersed single Ni site catalysts for nitrogen reduction toward electrochemical ammonia synthesis using N2 and H2O, *Small Methods*, 2020, **4**, 1900821.

122 H. Yang, Y. Liu, Y. Luo, S. Lu, B. Su and J. Ma, Achieving high activity and selectivity of nitrogen reduction via Fe–N3 coordination on iron single-atom electrocatalysts at ambient conditions, *ACS Sustainable Chem. Eng.*, 2020, **8**, 12809–12816.

123 R. Zhang, L. Jiao, W. Yang, G. Wan and H.-L. Jiang, Single-atom catalysts templated by metal–organic frameworks for electrochemical nitrogen reduction, *J. Mater. Chem. A*, 2019, **7**, 26371–26377.

124 F. Lü, S. Zhao, R. Guo, J. He, X. Peng, H. Bao, J. Fu, L. Han, G. Qi, J. Luo, X. Tang and X. Liu, Nitrogen-coordinated single Fe sites for efficient electrocatalytic N2 fixation in neutral media, *Nano Energy*, 2019, **61**, 420–427.

125 W. Zang, T. Yang, H. Zou, S. Xi, H. Zhang, X. Liu, Z. Kou, Y. Du, Y. P. Feng, L. Shen, L. Duan, J. Wang and S. J. Pennycook, Copper single atoms anchored in porous nitrogen-doped carbon as efficient pH-universal catalysts for the nitrogen reduction reaction, *ACS Catal.*, 2019, **9**, 10166–10173.

126 M. Qin, X. Li, G. Gan, L. Wang, S. Fan, Z. Yin and G. Chen, Boosting electrocatalytic nitrogen fixation with Co–N3 site-decorated porous carbon, *ACS Sustainable Chem. Eng.*, 2020, **8**, 13430–13439.

127 J. Li, S. Chen, F. Quan, G. Zhan, F. Jia, Z. Ai and L. Zhang, Accelerated dinitrogen electroreduction to ammonia *via* interfacial polarization triggered by single-atom protrusions, *Chem*, 2020, **6**, 885–901.

128 X. Liu, Y. Jiao, Y. Zheng, M. Jaroniec and S. Z. Qiao, Building up a picture of the electrocatalytic nitrogen reduction activity of rransition metal single-atom catalysts, *J. Am. Chem. Soc.*, 2019, **141**, 9664–9672.

129 J. M. McEnaney, A. R. Singh, J. A. Schwalbe, J. Kibsgaard, J. C. Lin, M. Cargnello, T. F. Jaramillo and J. K. Nørskov, Ammonia synthesis from N2 and H2O using a lithium cycling electrification strategy at atmospheric pressure, *Energy Environ. Sci.*, 2017, **10**, 1621–1630.

130 S. Liu, T. Qian, M. Wang, H. Ji, X. Shen, C. Wang and C. Yan, Proton-filtering covalent organic frameworks with superior nitrogen penetration flux promote ambient ammonia synthesis, *Nat. Catal.*, 2021, **4**, 322–331.

131 Y. Ren, C. Yu, X. Tan, X. Han, H. Huang, H. Huang and J. Qiu, Is it appropriate to use the Nafion membrane in electrocatalytic N2 reduction?, *Small Methods*, 2019, **3**, 1900474.

132 L. Shi, Y. Yin, S. Wang, X. Xu, H. Wu, J. Zhang, S. Wang and H. Sun, Rigorous and reliable operations for electrocatalytic nitrogen reduction, *Appl. Catal., B*, 2020, **278**, 119325.

133 S. Z. Andersen, V. Colic, S. Yang, J. A. Schwalbe, A. C. Nielander, J. M. McEnaney, K. Enemark-Rasmussen, J. G. Baker, A. R. Singh, B. A. Rohr, M. J. Statt, S. J. Blair, S. Mezzavilla, J. Kibsgaard, P. C. K. Vesborg, M. Cargnello, S. F. Bent, T. F. Jaramillo, I. E. L. Stephens, J. K. Norskov and I. Chorkendorff, A rigorous electrochemical ammonia synthesis protocol with quantitative isotope measurements, *Nature*, 2019, **570**, 504–508.

134 J. Choi, H.-L. Du, C. K. Nguyen, B. H. R. Suryanto, A. N. Simonov and D. R. MacFarlane, Electroreduction of nitrates, nitrites, and gaseous nitrogen oxides: A potential source of ammonia in dinitrogen reduction studies, *ACS Energy Lett.*, 2020, **5**, 2095–2097.

135 B. Hu, M. Hu, L. Seefe and T. L. Liu, Electrochemical dinitrogen reduction to ammonia by Mo2N: Catalysis or decomposition?, *ACS Energy Lett.*, 2019, **4**, 1053–1054.

136 Y. Zhao, R. Shi, X. Bian, C. Zhou, Y. Zhao, S. Zhang, F. Wu, G. I. N. Waterhouse, L. Z. Wu, C. H. Tung and T. Zhang, Ammonia detection methods in photocatalytic and electrocatalytic experiments: How to improve the reliability of NH3 production rates?, *Adv. Sci.*, 2019, **6**, 1802109.

137 R. Michalski, Applications of ion chromatography for the determination of inorganic cations, *Crit. Rev. Anal. Chem.*, 2009, **39**, 230–250.